Limitations of solid finite elements in transverse shear stress evaluation and the use of CUF 1D models as an efficient alternative

Taylor & Francis
Taylor & Francis Group

Mechanics of Advanced Materials and Structures

ISSN: 1537-6494 (Print) 1537-6532 (Online) Journal homepage: www.tandfonline.com/journals/umcm20

Limitations of solid finite elements in transverse shear stress evaluation and the use of CUF 1D models as an efficient alternative

Erasmo Carrera & Rodolfo Azzara

To cite this article: Erasmo Carrera & Rodolfo Azzara (2026) Limitations of solid finite elements in transverse shear stress evaluation and the use of CUF 1D models as an efficient alternative, Mechanics of Advanced Materials and Structures, 33:1, 2674854, DOI: 10.1080/15376494.2026.2674854

To link to this article: https://doi.org/10.1080/15376494.2026.2674854

Published online: 26 May 2026.

MECHANICS OF ADVANCED MATERIALS AND STRUCTURES
2026, VOL. 33, NO. 1, 2674854
https://doi.org/10.1080/15376494.2026.2674854

Taylor & Francis by informa

ORIGINAL ARTICLE

OPEN ACCESS Check for updates

Limitations of solid finite elements in transverse shear stress evaluation and the use of CUF 1D models as an efficient alternative

Erasmo Carrera and Rodolfo Azzara

MUL[2] Lab, Department of Mechanical and Aerospace Engineering, Politecnico di Torino, Torino, Italy

ABSTRACT

Although solid finite elements has become the most widely used standard modeling tool in structural mechanics, their use for accurate stress analysis is intrinsically limited by mesh quality, aspect ratio sensitivity, discretization strategy, and difficulties in preserving local equilibrium at the element level. Achieving reliable stress fields typically requires very fine meshes, especially in slender or thin-walled structures, leading to a dramatic increase in the number of degrees of freedom and, consequently, to a prohibitive computational cost. Moreover, the highly stretched solid elements that often arise in practical applications can further degrade stress accuracy and compromise the robustness of the analysis. To overcome these limitations, this work propose higher-order one-dimensional (1D) beam elements with full three-dimensional (3D) capabilities, developed within the Carrera Unified Formulation (CUF). The proposed models are derived from 3D elasticity through refined kinematic assumptions and enable the accurate evaluation of 3D stress distributions without the need for full 3D solid discretizations. Linear static analyses are carried out on representative benchmark problems, with particular attention to stress accuracy, sensitivity to element aspect ratio, mesh refinement requirements, and equilibrium preservation. The results clearly show that conventional solid formulations, as used in ABAQUS and COMSOL, are highly unreliable, remaining strongly affected by discretization choices, whereas the proposed CUF-based beam models provide accurate, robust, and computationally efficient solutions. In addition, solid elements also exhibit significant difficulties in ensuring shear stress equilibrium at the element level, further limiting their suitability for detailed stress analysis. Overall, this study underscores the role of higher-order CUF beam elements as an effective and reliable alternative to traditional solid formulations for accurate stress analysis, as well as a valuable tool for verification, particularly for shear stress evaluation.

ARTICLE HISTORY
Received 20 April 2026
Accepted 5 May 2026

KEYWORDS
Finite Element method; Carrera Unified Formulation; Solid Models; Aspect Ratio; High-order beam models; Stress

1. Introduction

Accurate stress prediction in both axial and shear components is a fundamental requirement in the analysis and design of modern engineering structures, especially when complex geometries, heterogeneous materials, and multiscale effects are involved. In this context, the finite element method (FEM) has become the standard computational tool, with three-dimensional (3D) solid elements representing the most general and widely adopted modeling approach due to their ability to describe arbitrary geometries and fully 3D stress states [1,2].

Despite their versatility and widespread use in commercial finite element (FE) codes, 3D solid formulations present several limitations that can significantly affect both computational efficiency and solution accuracy. In particular, obtaining reliable stress predictions generally requires very fine discretizations. Since stresses are obtained from derivatives of the displacement field, their accuracy is inherently lower than that of displacements and strongly dependent on mesh quality, element formulation, and discretization strategy. Reliable stress predictions typically require highly refined meshes, especially in regions characterized by localized stress concentrations. This leads to significant sensitivity to mesh refinement and can result in inaccurate stress distributions if insufficient discretization is used [3]. As a result, the number of degrees of freedom (DOFs) increases dramatically, leading to substantial computational costs and often making large-scale analyses and parametric studies computationally prohibitive [4].

A further critical aspect affecting the accuracy of solid finite element models is the quality of the mesh, particularly the element aspect ratio. In practical applications, especially when dealing with slender structures, meshes often include highly stretched elements with large aspect ratios. It is well established that such element distortions can significantly degrade the accuracy of the numerical solution, particularly in stress prediction. High aspect ratio elements may lead to

CONTACT Rodolfo Azzara rodolfo.azzara@polito.it MUL[2] Lab, Department of Mechanical and Aerospace Engineering, Politecnico di Torino, Corso Duca degli Abruzzi 24, 10129 Torino, Italy.

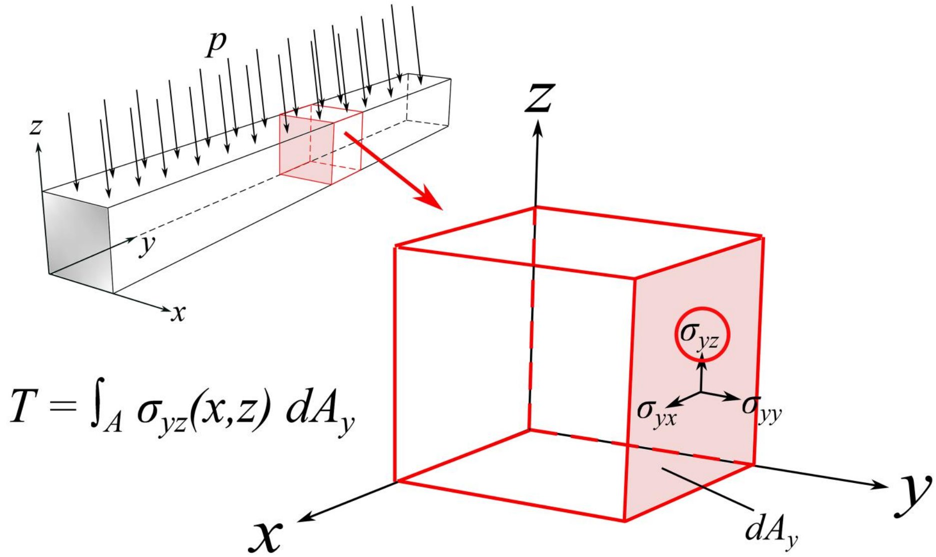

Figure 1. Stress components acting on the section of the element in a structure subjected to pressure loading.

poor interpolation of displacement fields and, consequently, to inaccurate stress distributions, even when the overall mesh density appears adequate [5–7].

Furthermore, several well-known numerical detrimental limitations affect solid finite elements and directly impact stress prediction. Among these, locking phenomena, such as shear and volumetric locking, are particularly critical. These effects can produce excessively stiff responses and spurious stress fields, especially in bending-dominated problems or in the analysis of slender structures, thus requiring further mesh refinement or specialized formulations to mitigate their influence. In addition, the presence of stress concentrations and boundary layers further exacerbates the limitations of solid models. Accurately capturing localized stress peaks requires extremely fine meshes in critical regions, which significantly increases computational effort and may still fail to yield reliable stress values in practical applications. To address these limitations, several numerical strategies have been developed to mitigate locking in solid finite elements. Classical techniques include reduced integration, which relaxes overly constrained kinematics that cause shear and volumetric locking, and selective or enhanced integration, in which shear and volumetric contributions are integrated with different quadrature rules to avoid spurious stiffness. Another widely adopted approach is the use of mixed displacement-pressure formulations, in which the hydrostatic pressure is treated as an independent field, thereby preventing volumetric locking in nearly incompressible regimes. Enhanced strain methods, such as the Enhanced Assumed Strain (EAS) [8,9] and Assumed Natural Strain (ANS) [10,11] techniques, further enrich the strain field to recover the correct deformation modes without introducing zero-energy instabilities in order to alleviate locking and improve numerical performance. These methods introduce additional formulation and algorithmic complexity, along with non-negligible computational overhead. Despite improving the performance of low-order solid elements, they do not remove the intrinsic dependence of stress accuracy on mesh refinement: fine discretizations remain necessary to obtain reliable stress fields, especially in the presence of strong gradients, localized effects, or severe mesh distortion. Moreover, some formulations require careful stabilization to maintain robustness in nonlinear analyses.

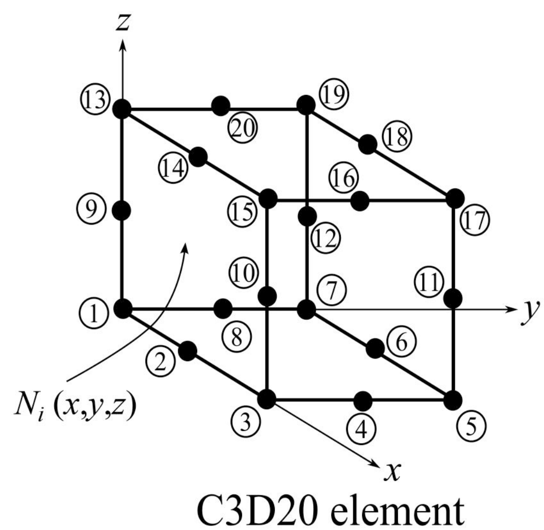

Figure 2. Example of a quadratic solid element.

In this context, the detrimental impact of locking on the performance of low-order solid elements has been extensively analyzed in the finite element literature. Early studies by Taylor et al. [12] demonstrated that fully integrated first-order hexahedral elements exhibit severe shear locking in bending-dominated problems, leading to overly stiff responses and poor convergence properties. Similar observations were reported by Hughes [13], who showed that inappropriate kinematic constraints in displacement-based formulations prevent the correct reproduction of bending modes, thereby generating spurious stress fields. The issue becomes even more pronounced in nearly incompressible elasticity or plasticity, where volumetric locking arises due to the inability of standard formulations to satisfy the incompressibility constraint. Seminal works by Nagtegaal et al. [14] and Markus and Hughes [15] documented that inappropriate interpolation and integration schemes can lead to spurious stiffness, particularly in bending-dominated and nearly incompressible problems, thereby motivating reduced/selective integration and mixed formulations Further analyses by Simo and Rifai [8] and Simo and Armero [9] established incompatible-mode and enhanced/mixed strain approaches as effective remedies for shear and volumetric locking in low-order solid elements. More recent reviews and benchmark studies have confirmed that locking remains a central issue in the use of solid and solid-shell elements for thin or bending-dominated structures, and that improved formulations can substantially enhance both displacement and stress predictions [16,17]. Collectively, these studies underline that locking is not merely a numerical inconvenience but a fundamental limitation of standard displacement-based solid elements, with direct consequences on stress accuracy and computational efficiency.

These concepts are also reflected in the implementation strategies adopted by the most used commercial finite element software, where locking mitigation is integrated directly within the element formulation and made available to the user through specific element families and integration schemes. In ABAQUS, for example, shear and volumetric locking are primarily addressed through selectively reduced integration and incompatible-mode formulations, as in the widely employed C3D8R element, which combines reduced integration with advanced hourglass control to prevent spurious zero-energy modes. For nearly incompressible materials, ABAQUS recommends hybrid mixed displacement-pressure elements (e.g. C3D8H, C3D20H), in which the pressure field is introduced as an independent variable to eliminate volumetric locking and improve the robustness of the solution. Similarly, COMSOL Multiphysics adopts similar principles: the software automatically switches to mixed formulations in incompressible or quasi-incompressible regimes, and employs selective reduced integration together with proprietary stabilization techniques to enhance the performance of low-order solid elements. While these implementations are effective in many practical scenarios, they do not completely eliminate the dependence of stress accuracy on mesh refinement, and fine discretizations remain necessary in the presence of strong stress gradients or boundary layers, where even stabilized solid formulations may struggle to reproduce accurate stress fields.

As an alternative, reduced-order structural models, such as one-dimensional (1D) beam theories, provide a computationally efficient framework for analyzing slender structures. Classical beam formulations, including the Euler-Bernoulli [18,19], de Saint-Venant [20,21], and Timoshenko [22] theories, offer substantial reductions in computational costs but remain inherently limited in their ability to reproduce complex 3D stress states. In recent decades, considerable research has focused on overcoming these limitations [23–25]. Numerous studies have shown that classical 1D structural theories can indeed be refined [26–28]. However, such improvements are typically problem-dependent [29]. For this reason, solid finite element models remain indispensable and are widely used in the literature to achieve high-fidelity structural analyses. As highlighted in the reference [30], solid formulations enable a comprehensive 3D evaluation of the displacement and stress fields, an essential capability in thermo-mechanical and electro-mechanical problems, where local effects induced by multi-physics coupling require detailed descriptions. 3D deformability is also crucial in structural dynamics, including applications such as vibrations of thin-walled components, rotordynamics, viscoelastic behavior, and wave propagation. In these contexts, classical 1D models often prove inadequate, while solid models can accurately capture complex phenomena such as shear deformation, nonstandard boundary conditions, and centrifugal stiffening. Similarly, in viscoelastic damping treatments, reliable stress predictions are essential, especially for thick layers. In composite structures, failure assessments are highly dependent on the accuracy of the strain and stress fields. The availability of a complete 3D stress state is therefore essential for reliable failure indices, especially in the presence of free-edge effects, matrix cracking, and localized damage.

In this work, a higher-order 1D beam methodology is proposed to address the limitations of standard 3D solid finite element models, with particular emphasis on the accurate evaluation of stress fields. The proposed approach enables accurate stress predictions without resorting to excessively refined 3D meshes, thereby reducing computational costs and avoiding the numerical issues that often

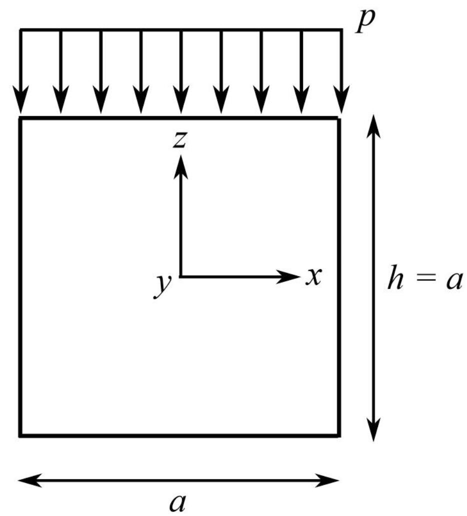

Figure 3. Representation of the isotropic square-section beam structure.

Table 1. Displacement values at the free end of the isotropic square-section beam structure using different ABAQUS and COMSOL models.

Model	AR	DOFs	u_z [m]
5×1×1 C3D20	20	204	−0.30
10×1×1 C3D20	10	384	−0.31
20×1×1 C3D20	5	744	−0.31
30×1×1 C3D20	3.33	1104	−0.32
100×1×1 C3D20	1	3624	−0.32
5×1×1 Q20	20	204	−0.30
10×1×1 Q20	10	384	−0.31
20×1×1 Q20	5	744	−0.31
30×1×1 Q20	3.33	1104	−0.32
100×1×1 Q20	1	3624	−0.32

arise in solid formulations. The methodology allows the construction of arbitrary-order 1D structural models that preserve the same physical 3D representation as a solid element. Notably, the proposed 1D models employ the same nodal degrees of freedom, three displacement components per node, as their solid counterparts. Within the Carrera Unified Formulation (CUF), higher-order beam theories have been systematically developed, offering a versatile and comprehensive framework for advanced structural modeling [31]. CUF employs index notation to express a wide range of structural theories within a single, compact formulation, enabling the straightforward development of refined models. The key idea is to enrich the beam kinematics by introducing additional interpolation functions, in addition to the standard finite element ones, to describe the cross-section deformation [32]. This enrichment enables accurate prediction of 3D stress states, strains, and transverse deformation modes without the computational burden associated with solid meshes. The CUF framework has been successfully applied across a wide range of engineering problems, including static analyses [33,34], dynamic response [35,36], micromechanics [37], thermo-elastic behavior [38], and aeroelastic formulations [39], among others.

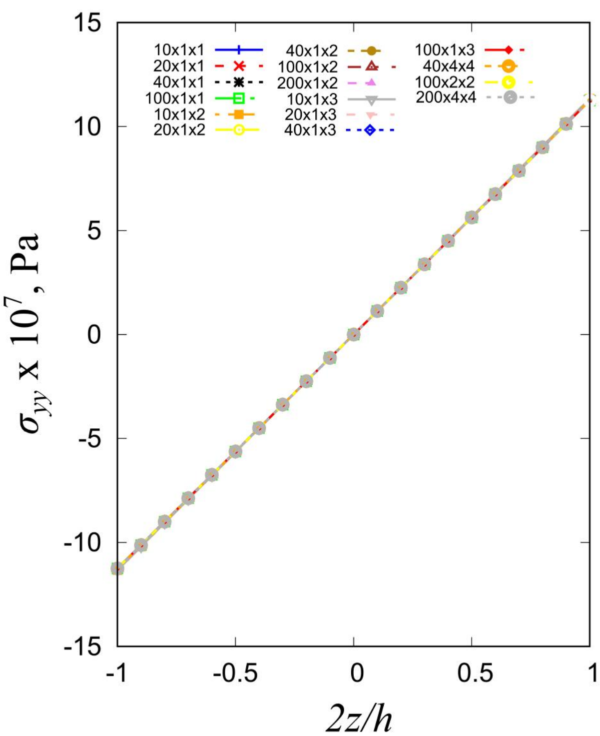

Figure 4. Through-the-thickness axial stress σ_{yy} distribution for the isotropic square compact beam at the midspan using ABAQUS.

The present work investigates the accuracy of stress predictions in compact and thin-walled structures using traditional 3D solid models with different discretization strategies. The analysis aims to highlight the intrinsic difficulties and limitations associated with these models, particularly in relation to mesh density and element aspect ratio, which can significantly affect the reliability of the computed stress fields. In particular, the study examines how variations in mesh refinement and element distortion influence the prediction of stress distributions, with special emphasis on the representation of stress distributions and peak values across the cross-section. These aspects are critical in static analyses, where accurate stress evaluation is required for reliable structural assessment. In addition, special attention is devoted to the difficulty of solid models in ensuring the local satisfaction of elastic equilibrium within each element or the resulting in each section of the structure, see Figure 1.

To address these issues, the results obtained with solid models are subsequently compared with those provided by higher-order 1D beam models based on the CUF. These models employ an enriched kinematic description of the

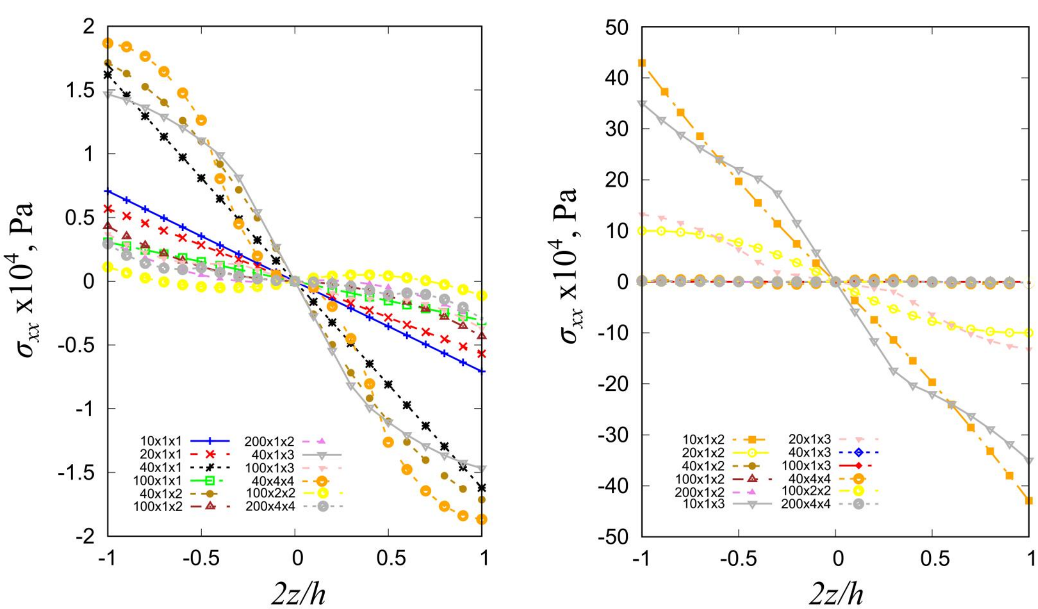

(a) FULL (b) RI

Figure 5. Through-the-thickness in-plane normal stress σ_{xx} distribution for the isotropic square compact beam at the midspan using ABAQUS.

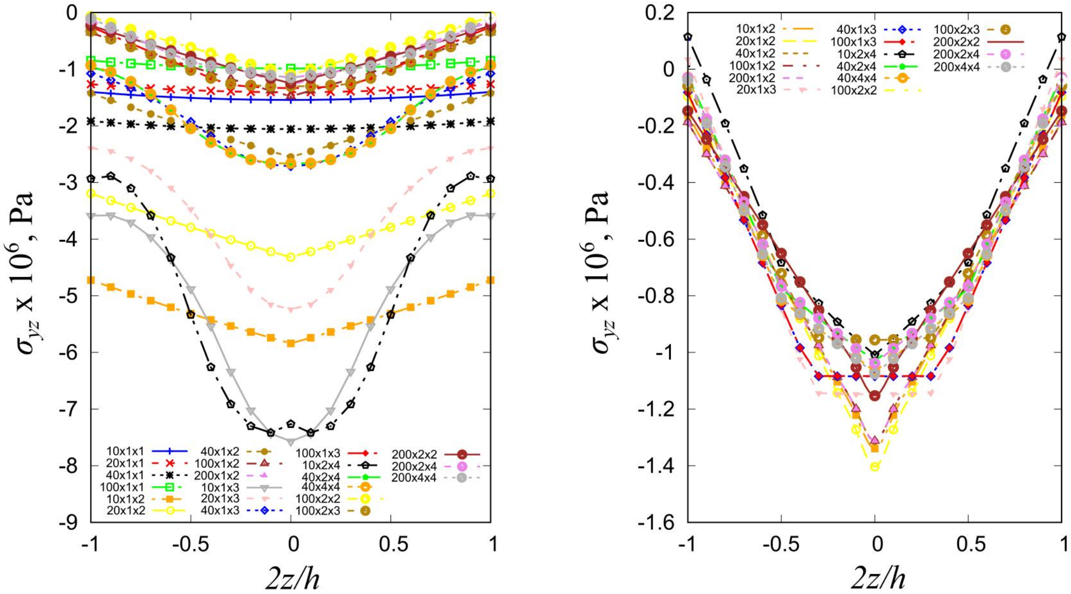

(a) FULL (b) RI

Figure 6. Through-the-thickness transverse shear stress σ_{yz} distribution for the isotropic square compact beam at the midspan using ABAQUS.

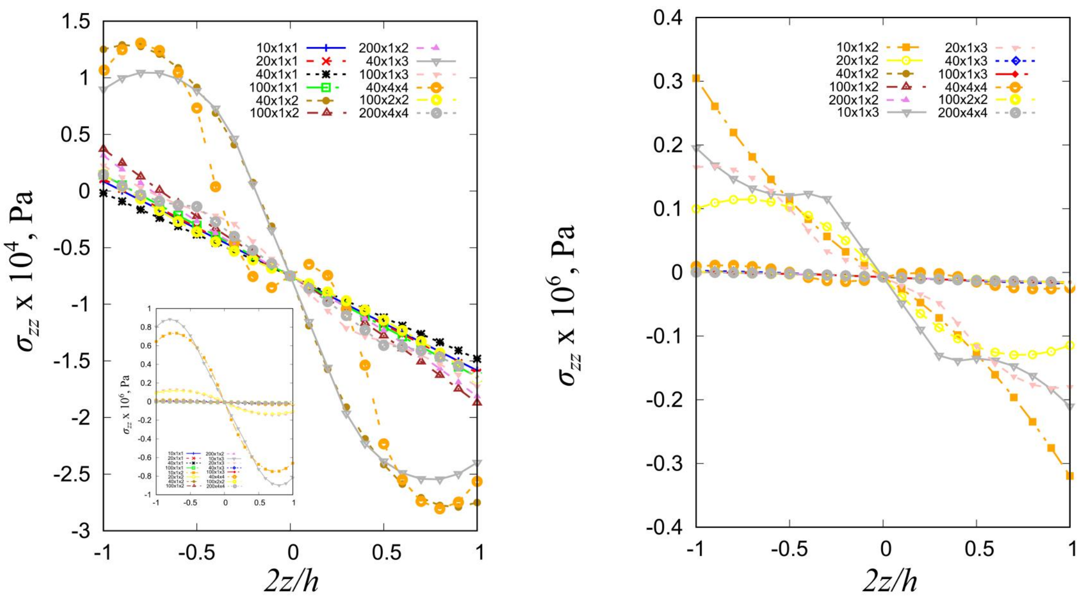

(a) FULL (b) RI

Figure 7. Through-the-thickness out-of-plane normal stress σ_{zz} distribution for the isotropic square compact beam at the midspan using ABAQUS.

cross-section, enabling the accurate evaluation of 3D stress states without the need for excessively refined meshes. This comparison between the two modeling approaches is carried out with the objective of demonstrating the robustness, accuracy, and computational efficiency of the proposed 1D formulation and how CUF-based models can effectively overcome the limitations of standard solid elements. Particularly, this 1D approach allows:

- to reduce sensitivity to mesh discretization and aspect ratio;
- to improve the consistency of the stress field and better satisfy local equilibrium conditions;
- to perform reliable predictions of stress distributions and peak values;
- to achieve these results with a significantly lower computational cost;
- to provide a reliable reference framework for the verification and validation of results obtained with other numerical tools.

The discussion emphasizes not only the computational benefits but also the ability of higher-order 1D approaches to serve as efficient and accurate tools for structural analysis, contributing to the development of robust and versatile

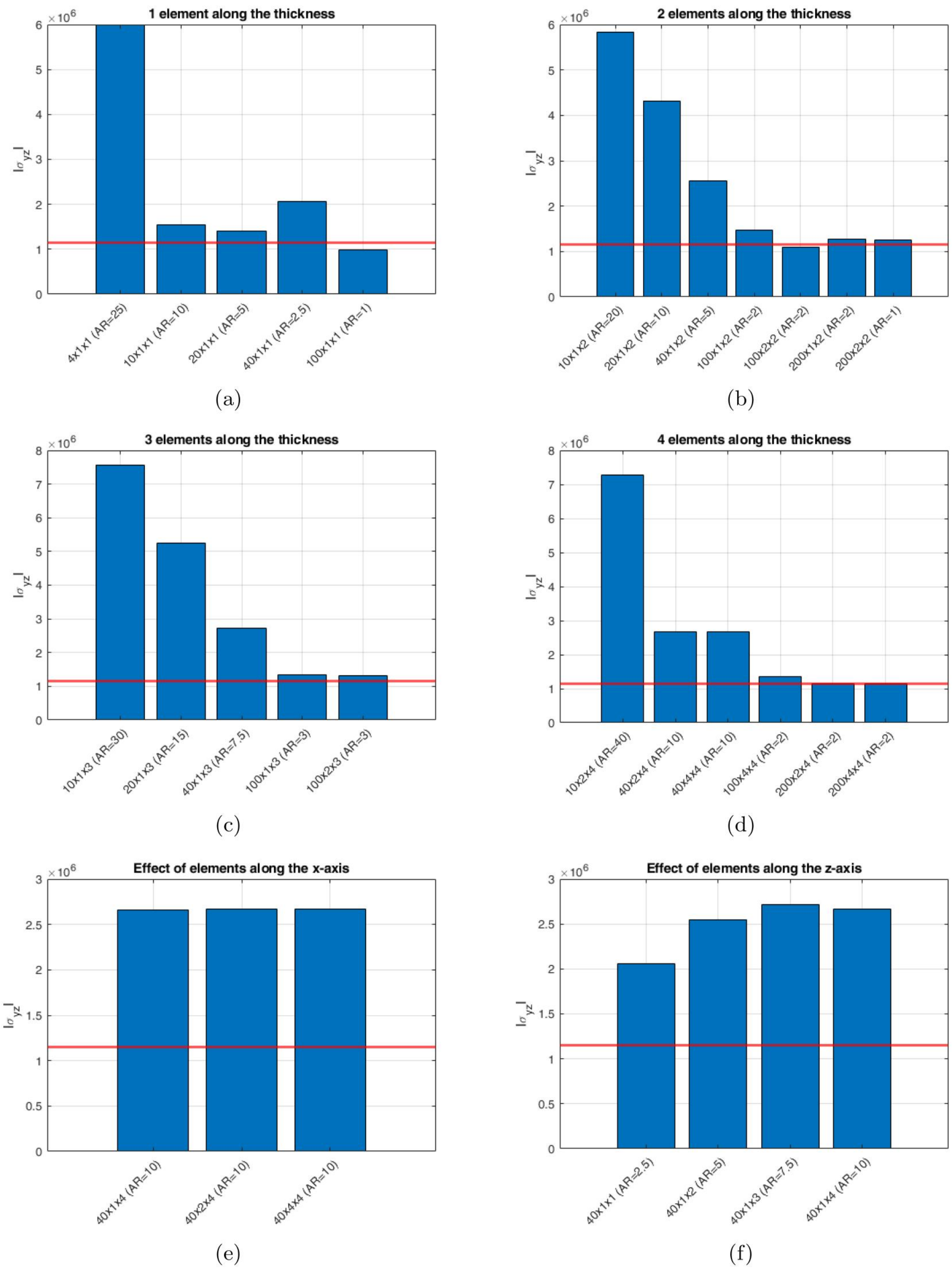

Figure 8. Effect of the element aspect ratio in ABAQUS solid models. The red line represents the reference value (200×4×4 C3D20 model). Isotropic square-section beam structure.

Table 2. Resultant comparison between ABAQUS and COMSOL solutions at the one-quarter span of the square-section beam structure. The percentage error reported for each model is calculated with respect to the theoretical sectional shear resultant of −112.50 N at this location.

Model	AR	DOFs	Resultant T [N]	Error %
ABAQUS—FULL	10	10995	−298.38	165.9
ABAQUS—FULL	2	54195	−122.34	8.75
ABAQUS—RI	2	54195	−111.66	−0.75
COMSOL	1.5	24687	−123.16	9.47
COMSOL	1.2	90375	−110.89	−1.43
COMSOL	1.2	232839	−114.44	1.72

Table 3. Resultant comparison between ABAQUS and COMSOL solutions at the midspan of the square-section beam structure. The percentage error reported for each model is calculated with respect to the theoretical sectional shear resultant of −75.00 N at this location.

Model	AR	DOFs	Resultant T [N]	Error %
ABAQUS—FULL	10	10995	−199.5	166.00
ABAQUS—FULL	2	54195	−82.41	9.88
ABAQUS—RI	2	54195	−74.95	−0.67
COMSOL	1.5	24687	−82.30	9.73
COMSOL	1.2	90375	−77.96	3.95
COMSOL	1.2	232839	−76.29	1.72

modeling strategies for next-generation engineering applications. The effectiveness of the proposed methodology is demonstrated through a systematic comparison with results obtained from different commercial 3D solid FE models.

The paper is organized as follows: (i) Section 2 introduces the solid formulation and presents some numerical results that illustrate the intrinsic limitations of these element in accurately evaluating the stress distributions; (ii) Section 3 presents the higher-order beam formulations and provides numerical results in order to demonstrate how the proposed 1D beam models effectively overcome the shortcomings of solid elements; (iii) finally, conclusions are presented in Section 4.

Table 4. Resultant comparison between ABAQUS and COMSOL solutions at the three-quarter span of the square-section beam structure. The percentage error reported for each model is calculated with respect to the theoretical sectional shear resultant of −37.50 N at this location.

Model	AR	DOFs	Resultant T [N]	Error %
ABAQUS—FULL	10	10995	−99.47	165.25
ABAQUS—FULL	2	54195	−40.78	8.75
ABAQUS—RI	2	54195	−37.22	−0.75
COMSOL	1.5	24687	−41.05	9.47
COMSOL	1.2	90375	−36.96	−1.44
COMSOL	1.2	232839	−38.15	1.73

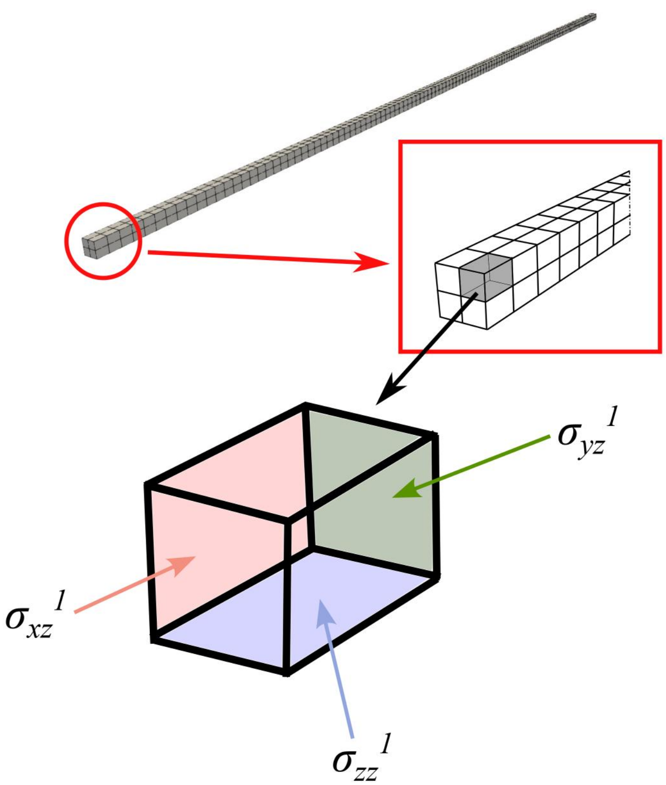

Figure 9. Local element for the evaluation of the equilibrium in the isotropic square-section beam structure.

2. Solid finite element formulation

According to the FEM, the 3D displacement field of a solid element in static conditions can be expressed as:

$$\boldsymbol{u}(x, y, z) = N_i(x, y, z)\boldsymbol{q}_i, \qquad i = 1, \ldots, N_n^{3D} \tag{1}$$

where N_i represent the shape functions, $\boldsymbol{q}_i$ are the nodal displacement vector, N_n^{3D} is the number of nodes per element, and the index i implies summation.

In standard 3D solid formulation, the same interpolation strategy is adopted along all spatial directions. In this work, both the commercial software ABAQUS and COMSOL are used to perform 3D solid analyses. Specifically, the following elements are used: the 20-node quadratic serendipity hexahedral solid element with full integration (C3D20), the 20-node quadratic serendipity hexahedral solid element with reduced integration (C3D20R), and the 20-node quadratic serendipity hexahedral solid element (Q20) are adopted. Figure 2 illustrates the quadratic solid element employed in this study. All these elements share the same nodal layout and numbering scheme, consisting of 20 nodes: 8 corner

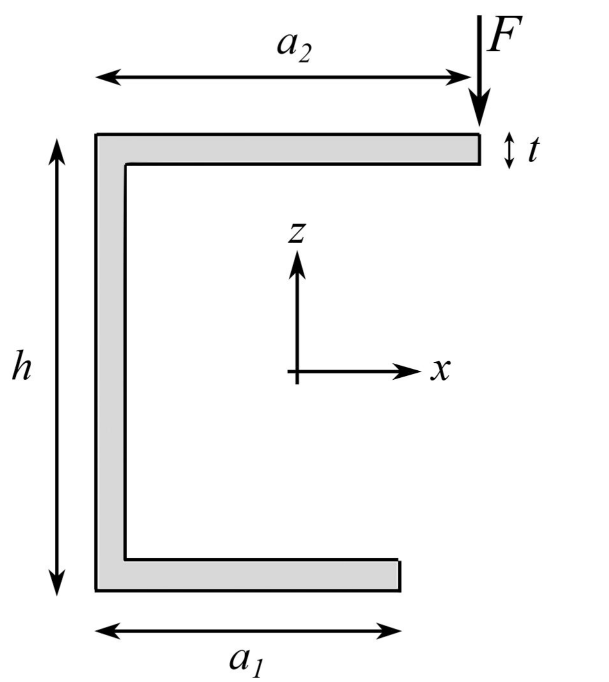

Figure 10. Cross-section geometry of the unsymmetric open-section beam structure.

Table 5. Equilibrium evaluation using ABAQUS and COMSOL at the considered single element. Model discretization of the square-section beam structure: 125×2×2 elements adopted in the three directions. The percentage error reported in the table is computed with respect to the theoretical pressure resultant of −0.60 N applied to this element.

Model	$T_{\sigma_{xz}^1}$	$T_{\sigma_{xz}^2}$	$T_{\sigma_{yz}^1}$	$T_{\sigma_{yz}^2}$	$T_{\sigma_{zz}^1}$	$T_{\sigma_{zz}^2}$	Resultant [N]	Error %
ABAQUS—FULL	0.0088	0.0000	−0.3705	−0.0351	−0.3000	−0.6901	−0.72	19.44
ABAQUS—RI	0.0066	0.0000	−0.3000	0.0000	−0.3000	−0.6374	−0.63	5.13
COMSOL	0.0088	−0.0024	−0.3746	−0.0352	−0.2893	−0.6426	−0.68	13.59

Table 6. Displacement values at the free end of the C-section beam using different ABAQUS and COMSOL models.

Model	AR	DOFs	$u_z \times 10^{-2}$ [m]
50 C3D20	50	1284	−1.644
460 C3D20	100	8013	−1.663
250 C3D20	10	6084	−1.664
2300 C3D20	20	37893	−1.680
500 C3D20	5	12084	−1.666
4600 C3D20	10	75243	−1.681
9200 C3D20	5.55	149943	−1.682
13800 C3D20	5.55	224643	−1.683
18400 C3D20	5.55	299343	−1.683
196 Q20	17.86	4650	−1.669
918 Q20	4.80	20952	−1.671
7650 Q20	2.20	166464	−1.681
12060 Q20	1.25	259749	−1.683

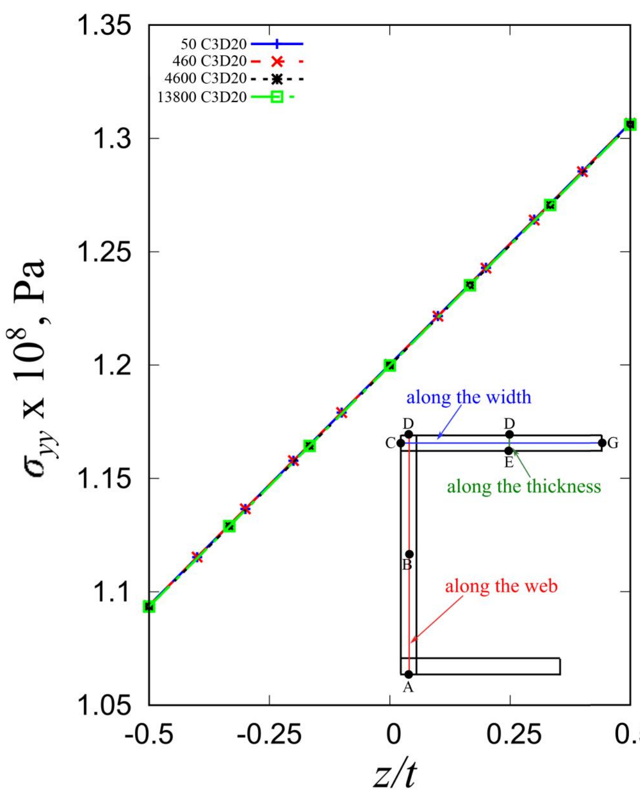

Figure 11. Through-the-thickness axial stress σ_{yy} distribution C-section beam at the midspan using ABAQUS.

nodes located at the vertices of the hexahedron and 12 mid-edge nodes positioned at the centers of each edge.

While this approach is convenient from an implementation standpoint, it becomes inefficient when the structure exhibits highly different characteristic dimensions. In particular, for slender or thin-walled components, the displacement field can not be selectively enriched along the most critical directions, leading to inaccurate stress predictions unless very fine meshes are used. This limitation is particularly critical in static analyses, where the accurate evaluation of stress fields, especially shear stresses, is essential. In such cases, solid elements often require a large number of elements across the cross-section to accurately capture stress distributions, resulting in a significant increase in computational cost.

The governing equations for static analyses are derived from the Principle of Virtual Displacements (PVD):

$$\delta L_{int} = \delta L_{ext} \tag{2}$$

where δL_{int} represents the internal virtual work due to the elastic forces, δL_{ext} stands for the work of external forces, and δ denotes virtual variations. Specifically, these components can be expressed in the form of 3×3 Fundamental Nuclei (FNs). The FNs are independent of the theory approximation and may be expanded against N_i shape functions to derive the final matrices and vectors. The variations of the internal and external work are expressed in terms of FNs of the stiffness matrix and external force vector as follows:

$$\begin{aligned} \delta L_{int} &= \delta \boldsymbol{q}_j^{\mathrm{T}} \boldsymbol{K}^{ij} \boldsymbol{q}_i \\ \delta L_{ext} &= \delta \boldsymbol{q}_j^{\mathrm{T}} \boldsymbol{p}_j \end{aligned} \tag{3}$$

where $\boldsymbol{\epsilon}$ and $\boldsymbol{\sigma}$ are the strain and stress vectors, respectively, and $\boldsymbol{p}$ stands for the nodal loading vector.

By introducing the linear elastic constitutive relation, the equilibrium equations can be written as follows:

$$\boldsymbol{K}\boldsymbol{q} = \boldsymbol{F} \tag{4}$$

In a compact notation, the FNs of the stiffness matrix are expressed as:

$$\boldsymbol{K}^{ij} = \int_V N_j(x, y, z) \boldsymbol{b}^{\mathrm{T}} \boldsymbol{C} \; N_i(x, y, z) \boldsymbol{b} \; dV \tag{5}$$

where $\boldsymbol{b}$ denotes a linear differential operator and $\boldsymbol{C}$ represents the material's linear elastic matrix. Although the matrix $\boldsymbol{K}$ contains nine terms, only two have a different structure. Consider the following two terms in the case of the solid:

$$\begin{aligned} \boldsymbol{K}_{xx}^{ij} &= (\lambda + 2G) \int_V N_{i,x}(x, y, z) N_{j,x}(x, y, z) \; dV \\ &\quad + G \int_V N_{i,z}(x, y, z) N_{j,z}(x, y, z) \; dV + \\ &\quad + G \int_V N_{i,y}(x, y, z) N_{j,y}(x, y, z) \; dV \\ \boldsymbol{K}_{xy}^{ij} &= \lambda \int_V N_{i,x}(x, y, z) N_{j,y}(x, y, z) \; dV \\ &\quad + G \int_V N_{i,y}(x, y, z) N_{j,x}(x, y, z) \; dV \end{aligned} \tag{6}$$

where G stands for the shear modulus and λ is the Lamé coefficient vector. From Eq. 6, it becomes evident that the construction of the stiffness matrix in solid formulations relies on a full 3D volume integration. This requirement has direct consequences on both the computational cost and the numerical behavior of the elements. In particular, solid formulations are inherently sensitive to the element aspect ratio, a limitation that becomes especially pronounced in slender, thin-walled or composite structures. Achieving accurate stress predictions typically demands elements with low aspect ratios, which in turn necessitates highly refined meshes. These constraints significantly increase the computational effort and may hinder the ability to capture complex 3D effects unless substantial mesh refinement is employed.

Once the equilibrium equations are solved, the evaluation of the stress field becomes a central aspect of the analysis. In solid elements, stresses are computed from the displacement field as:

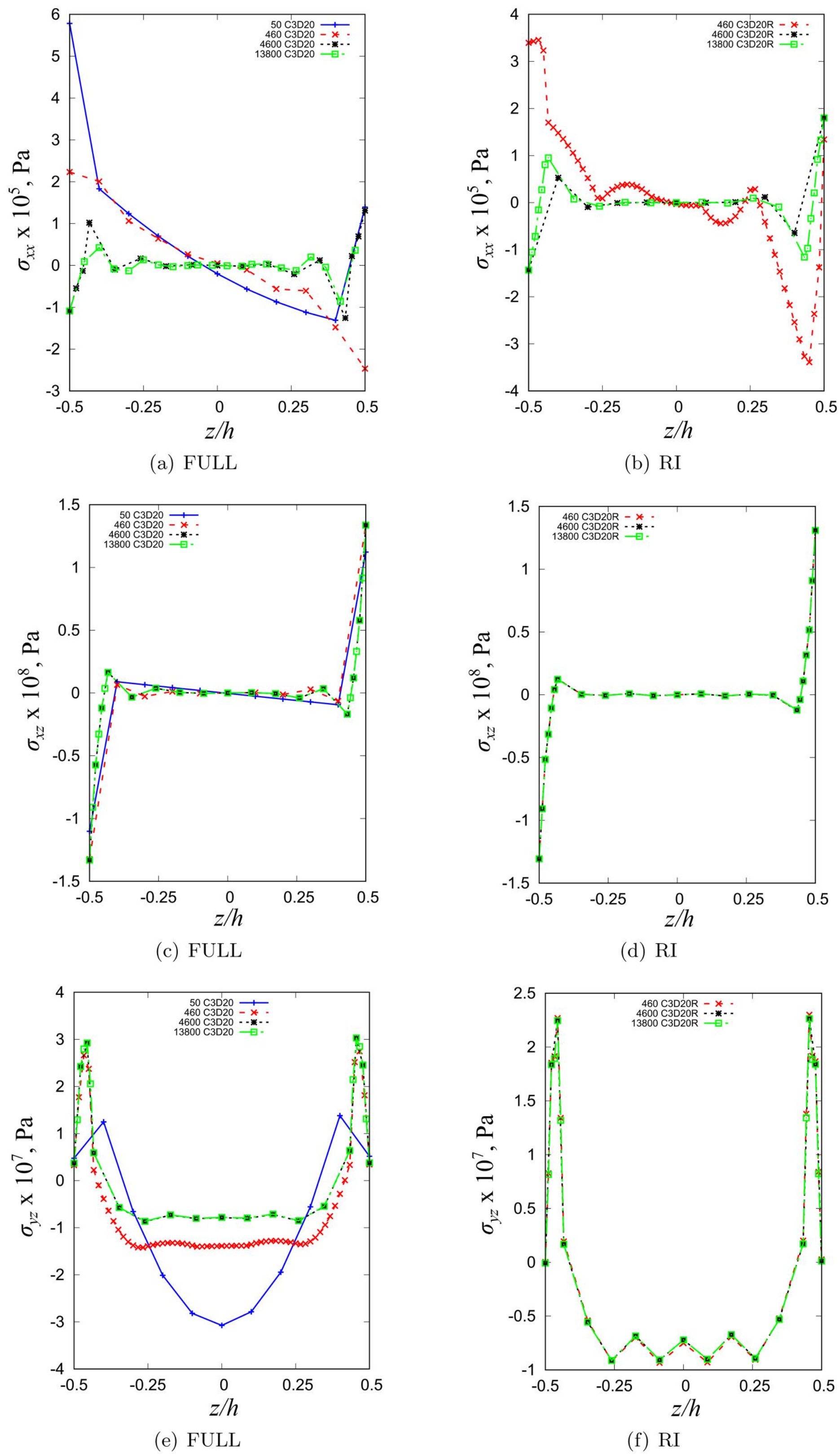

Figure 12. Stress distributions for the isotropic C-section beam at the midspan of the structure and along the web using ABAQUS quadratic solid models.

$$\boldsymbol{\sigma} = \boldsymbol{C\epsilon} = \boldsymbol{Cb}N_i\boldsymbol{q}_i \tag{7}$$

in which $\boldsymbol{C}$ contains the coefficients of the material, and $\boldsymbol{b}$ stands for the linear differential operator. Consequently, the quality of the stress field depends strictly on the accuracy of the displacement interpolation. With coarse meshes or high aspect ratio elements, typical of slender structures, the strain field can be approximated inaccurately. This can lead to inaccurate stress distributions, spurious stiffness effects, and

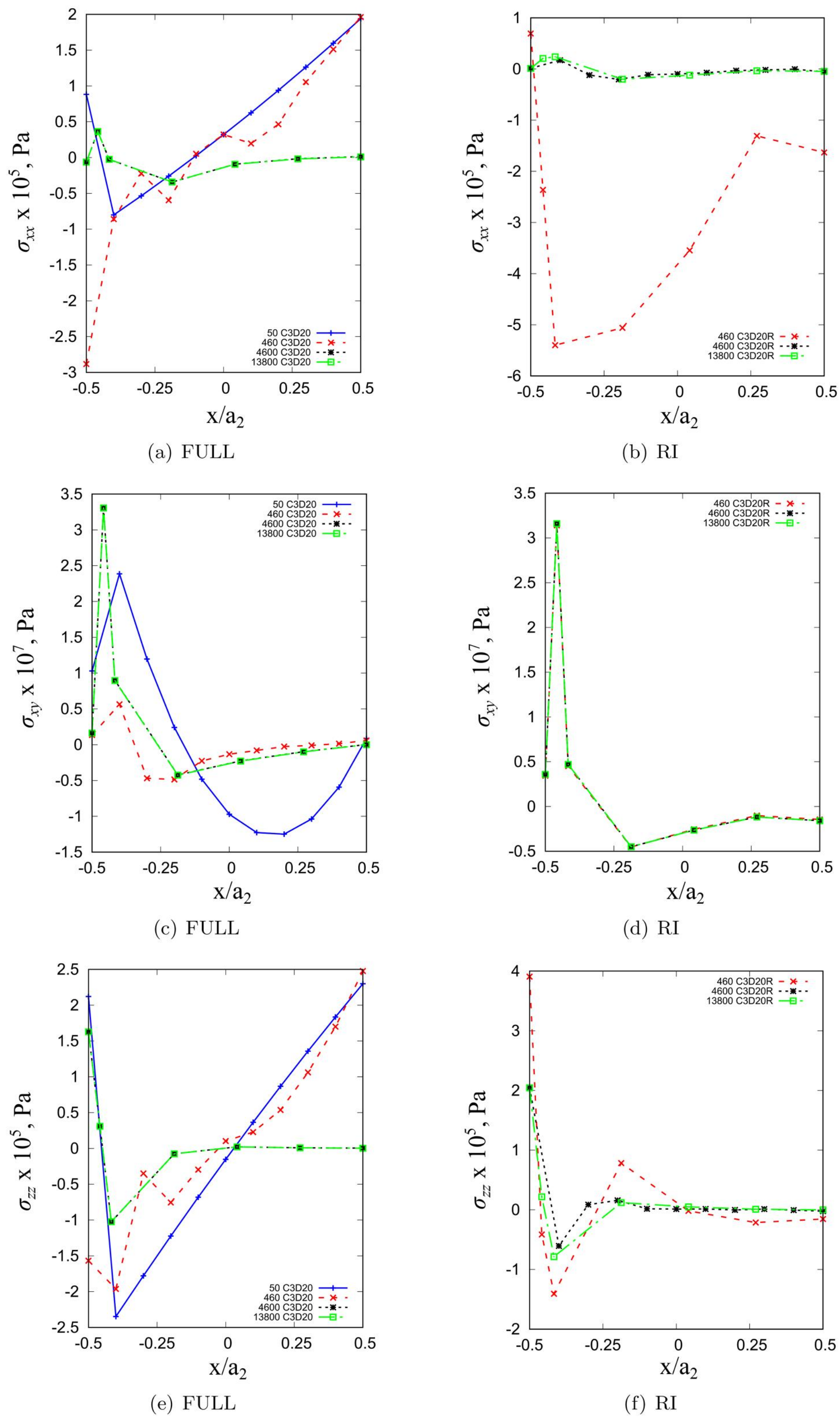

Figure 13. Stress distributions for the isotropic C-section beam at the midspan and along the width of the top flange using ABAQUS.

unreliable predictions of peak stresses. These limitations are particularly critical when analyzing stress distributions along the beam cross-section, where large variations can occur even when considering simple geometries or under simple loading conditions.

2.1. Numerical results using 3D solid FEs

This section examines the static response and stress distribution of both compact and thin-walled isotropic structures. The objective is to highlight the inherent limitations and

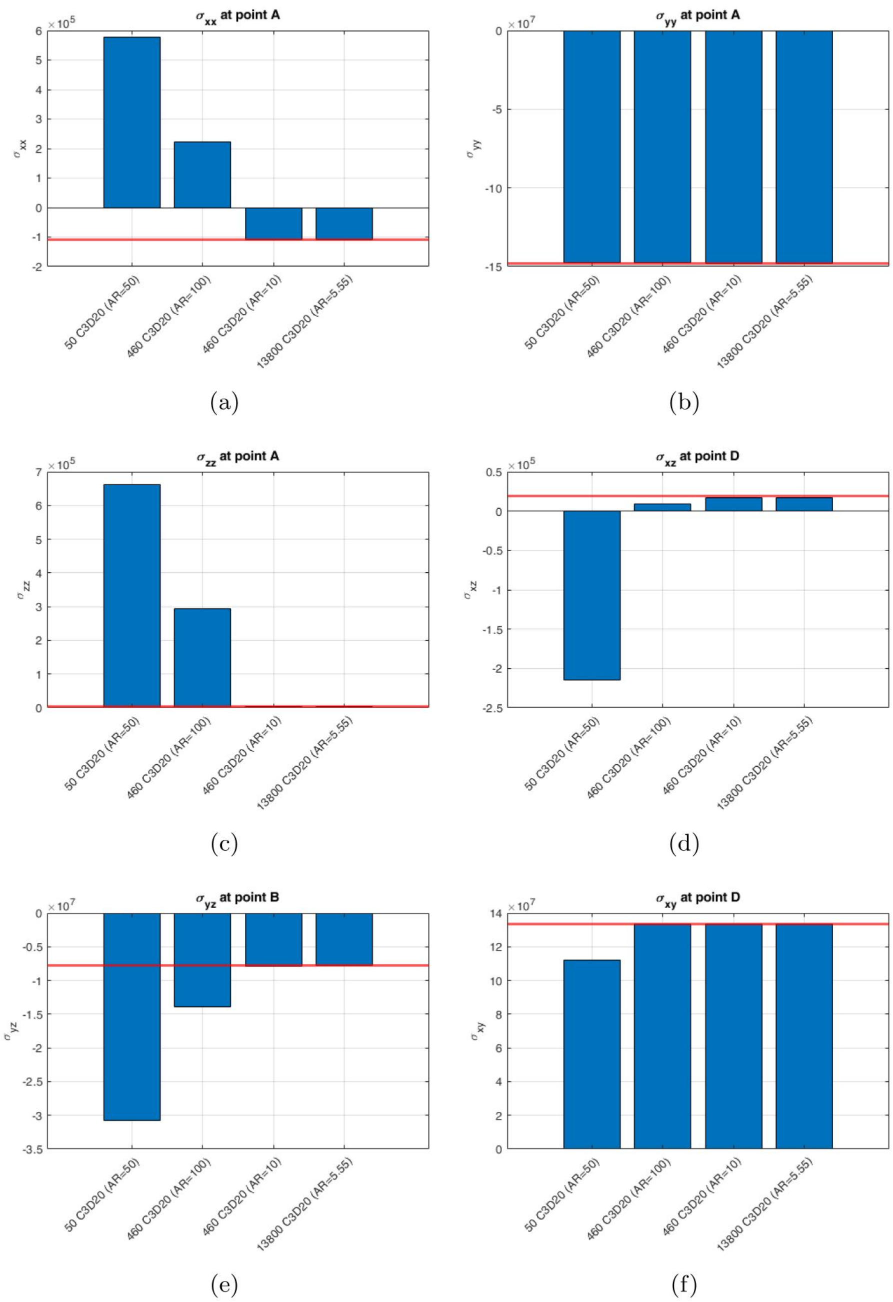

Figure 14. Effect of the element aspect ratio in ABAQUS solid models evaluating the stress along the web in the C-section beam. The red line represents the reference value (300×4×3 C3D20 model).

numerical difficulties associated with quadratic solid elements commonly employed in commercial finite element software, such as ABAQUS and COMSOL. The analysis first relies exclusively on solid elements in order to clearly expose their shortcomings. The results, reported in the following figures and table, include the computed structural responses along with the corresponding number of degrees of freedom and the element aspect ratio. For clarity, the aspect ratio is defined as the ratio between the longest and the shortest side of an individual element ($\mathrm{AR} = \frac{\text{longest side}}{\text{shortest side}}$), and the reported value is the maximum in the structure. In the following analysis, the discretization of each model is defined as: $\mathrm{n_{eley}}$ x $\mathrm{n_{elex}}$ x $\mathrm{n_{elez}}$, where $\mathrm{n_{ele}}$ indicates the number of elements along each direction.

2.1.1. Isotropic square compact beam

The first case considers a cantilever metallic compact beam with a square cross-section subjected to pressure loading. Figure 3 depicts the reference system and geometric parameters. The section dimension is 0.01 m, with a span-to-height ratio, L/h, equal to 100, whereas the material properties are the following: $E = 70\,\mathrm{GPa}$, and $\nu = 0.33$. A pressure $p = 15{,}000\,\mathrm{Pa}$ is applied to the upper surface along the entire length of the beam. The static response of this slender beam is analyzed by evaluating its stress distributions along the thickness. Various quadratic solid models both in ABAQUS and COMSOL were considered.

Table 1 shows the convergence analysis on the displacement at the free end for various solid models, including the

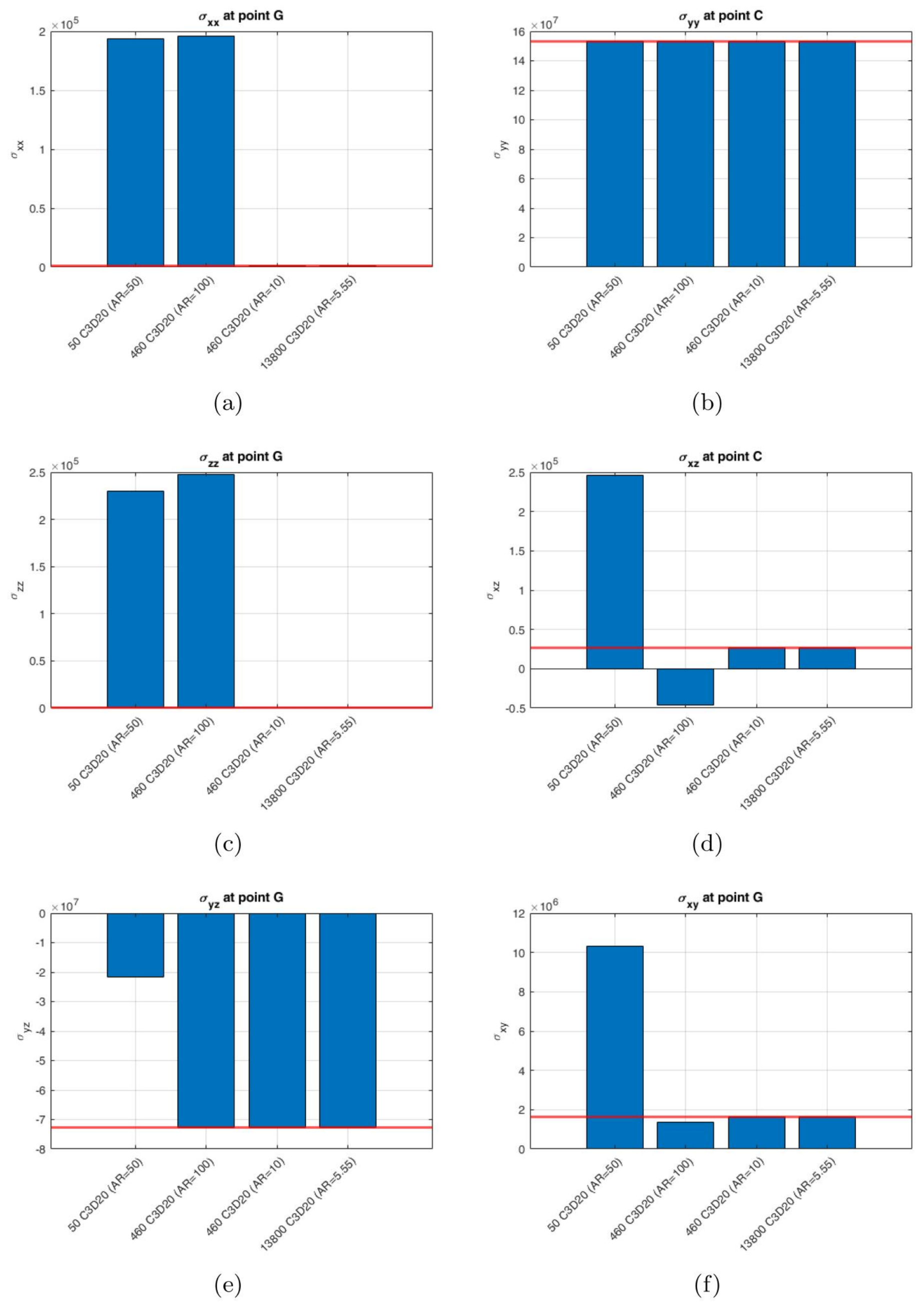

Figure 15. Effect of the element aspect ratio in ABAQUS solid models evaluating the stress along the width in the C-section beam. The red line represents the reference value (300×4×3 C3D20 model).

corresponding DOFs and AR values. The results clearly show that the aspect ratio has a non-negligible influence on the displacement field. Accordingly, the converged displacement value is obtained using at least a mesh configuration with AR = 3.33, which provides a sufficiently stable response.

Figures 4, 5, 6, and 7 illustrate the distributions of the normal stress along the beam axis, σ_{yy}, the normal stress in the in-plane section, σ_{xx}, the shear stress in the section, σ_{yz}, and the normal stress through the thickness, σ_{zz}, respectively. Each figure compares different solid models and integration strategies, i.e. with reduced integration (RI) or full (FULL), showing the convergence behavior obtained by varying the number of quadratic solid elements along the three spatial directions. To avoid redundancy in the presentation of similar plots and tables, full convergence analyses are reported only for the ABAQUS simulations. For COMSOL, only the converged values, or a limited selection of representative solid models, are included, mainly to highlight the numerical issues encountered also with this tool as well.

The results clearly highlight the significant difficulties of solid models in achieving convergence in the stress distributions, particularly for the out-of-plane components. While the axial stress component converges rapidly even for relatively high aspect ratio values, the other stress fields exhibit

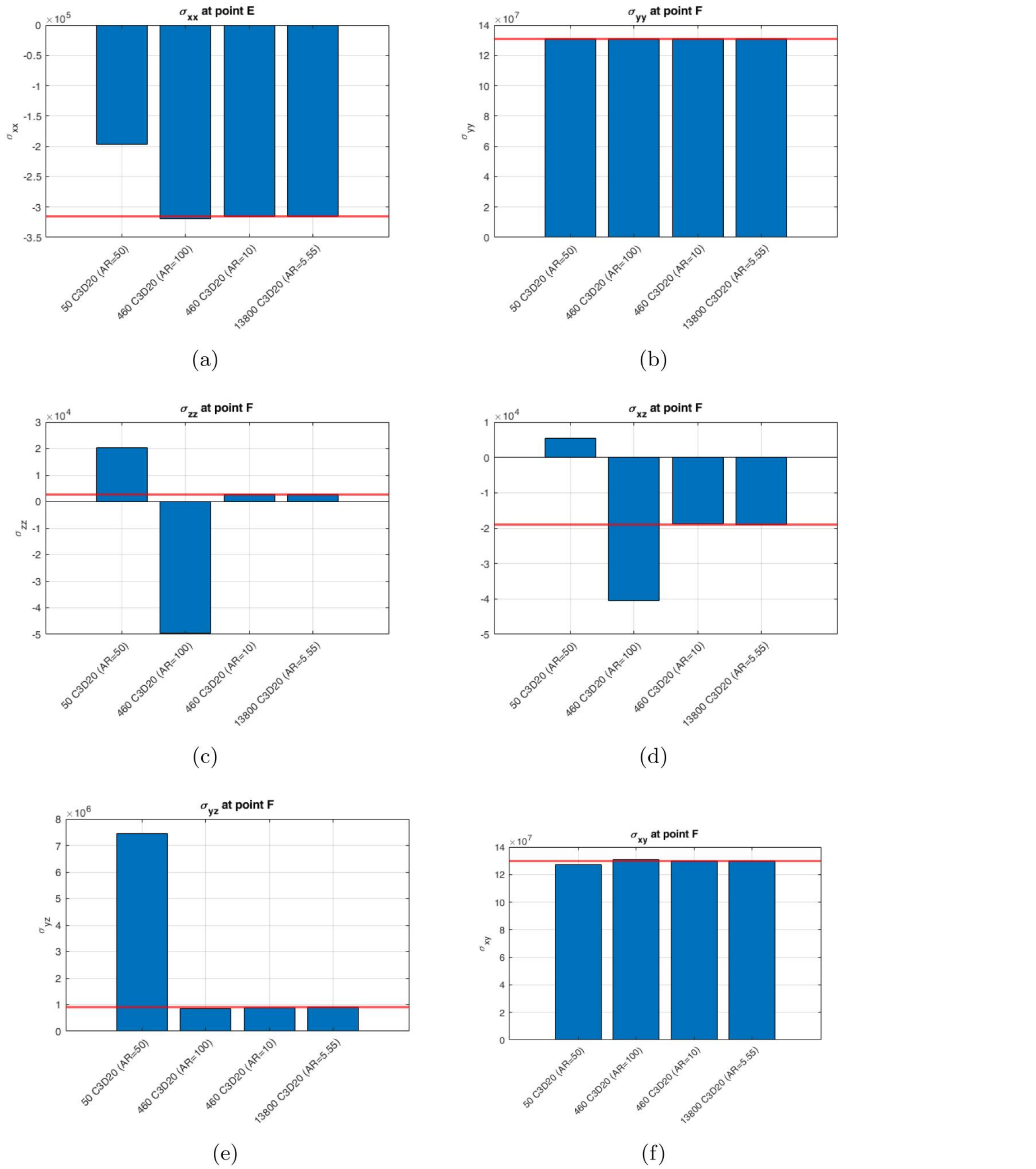

Figure 16. Effect of the element aspect ratio in ABAQUS solid models evaluating the stress along the thickness in the C-section beam. The red line represents the reference value (300×4×3 C3D20 model).

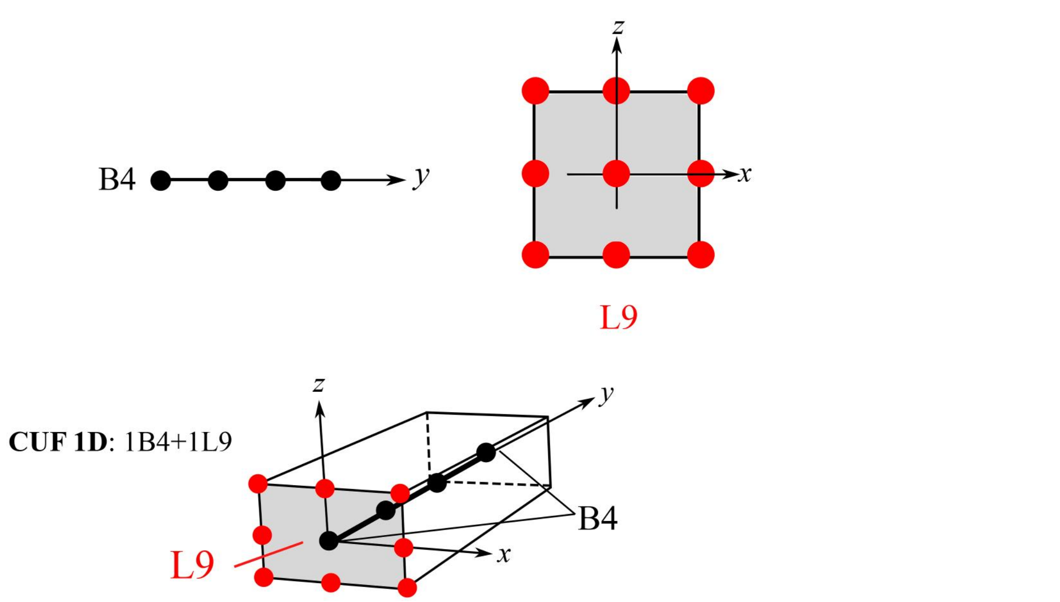

Figure 17. Example of a CUF 1D model.

Table 7. Displacement values using CUF 1D models for the isotropic cantilever beam with square cross-section.

Model	AR	DOFs	u_z [m]
5B4 + 1LE9	20	432	−0.31
10B4 + 1LE9	10	837	−0.32
10B4 + 1LE16	10	1488	−0.32
20B4 + 1LE9	5	1647	−0.32
30B4 + 1LE9	3.33	2457	−0.32

Table 8. Resultant comparison of CUF models at the one-quarter span of the square-section beam. The percentage error reported for each model is calculated with respect to the theoretical sectional shear resultant of −112.50 N at this location.

Model	AR	DOFs	Resultant T [N]	Error %
30B4 + 2LE16	10	5124	−112.38	−0.11
100B4 + 2LE16	2	25284	−112.47	−0.03

Table 9. Resultant comparison of CUF 1D models at the midspan of the square-section beam structure. The percentage error reported for each model is calculated with respect to the theoretical sectional shear resultant of −75.00 N at this location.

Model	AR	DOFs	Resultant T [N]	Error %
30B4 + 2LE16	10	5124	−76.36	1.81
100B4 + 2LE16	2	25284	−75.07	0.09

Table 10. Resultant comparison of CUF 1D models at the three-quarter span of the square-section beam structure. The percentage error reported for each model is calculated with respect to the theoretical sectional shear resultant of −37.50 N at this location.

Model	AR	DOFs	Resultant T [N]	Error %
30B4 + 2LE16	10	5124	−37.47	−0.08
100B4 + 2LE16	2	25284	−37.48	−0.05

Figure 18. Deformed configuration of the isotropic cantilever beam with square cross-section subjected to pressure loading.

a marked sensitivity to both mesh refinement and aspect ratio of the solid elements. Convergent solutions for these components are obtained only for very low AR values and, therefore, highly refined meshes. Such stringent requirements inevitably lead to computationally demanding models, as a significant increase in the number of quadratic solid elements is necessary to accurately capture the through-the-thickness stress trends. It is also worth noting that using reduced integration generally promotes faster convergence of stresses, mitigating, though not eliminating, the detrimental effects associated with high aspect ratios. Figure 8 further highlights the detrimental effect of the element aspect ratio on solid FEs in the evaluation of transverse shear stress peaks. The bar charts include convergence studies performed by varying the number of elements along the y-axis, for different discretizations through the thickness, as well as additional analyses assessing the influence of the number of elements along the x- and z-directions. As the AR increases, the solid formulations progressively lose accuracy in capturing the local stresses, leading to inaccurate peak values, particularly for the transverse shear stress component.

Tables 2, 3, and 4 compare the shear resultant (T) computed at different cross-sections of the structure for the various solid models. The results reveal significant percentage errors compared to the theoretical applied force, with discrepancies varying not only from one solid formulation to another, but also from section to section along the structure. This variability makes it challenging to identify consistent corrective factors, which are typically adopted in industrial practice. The observed results confirms that, even when

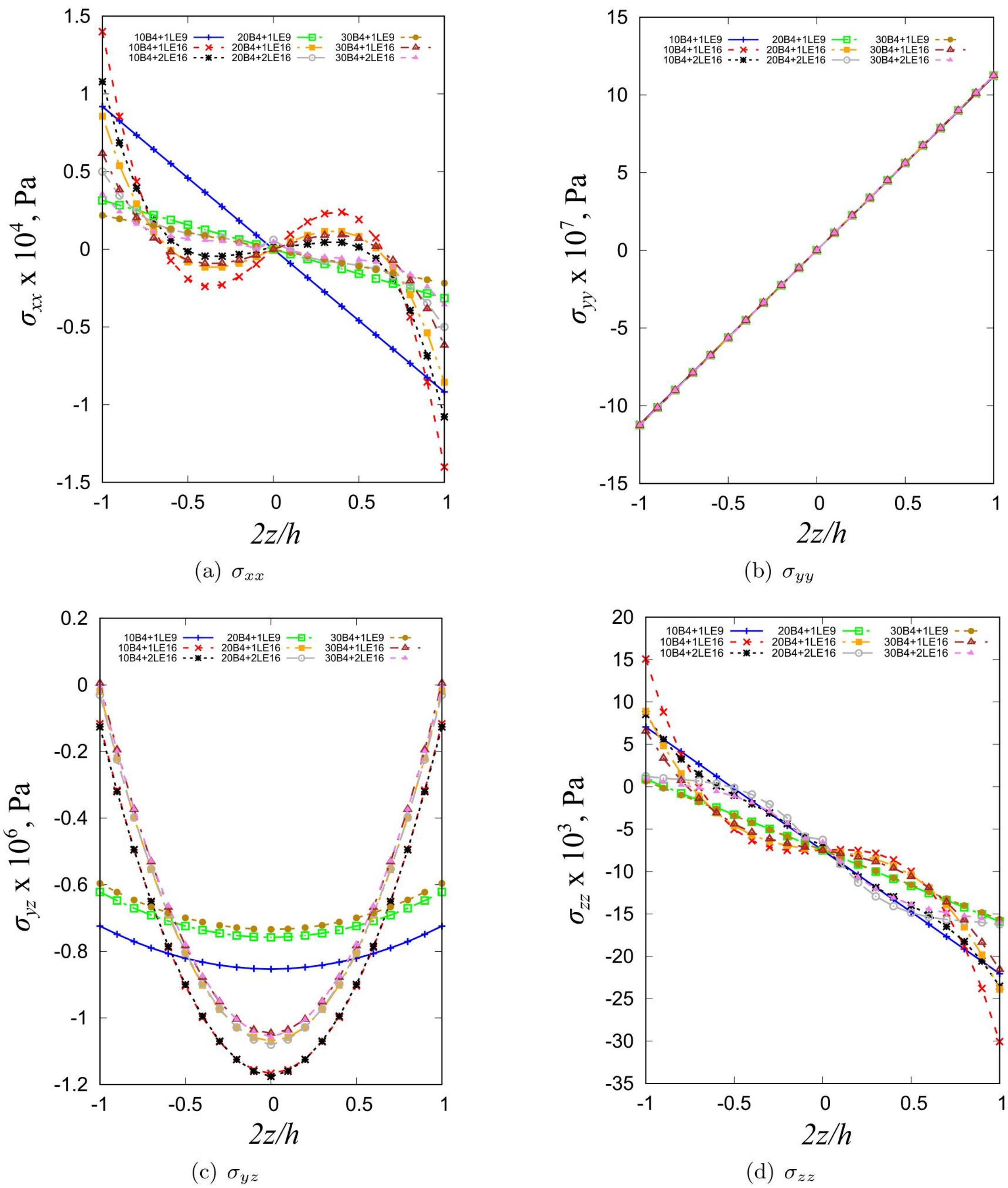

(a) σ_{xx}

(b) σ_{yy}

(c) σ_{yz}

(d) σ_{zz}

Figure 19. Convergence analysis on through-the-thickness stress distributions for the isotropic square compact beam at the midspan using CUF 1D models.

convergence is achieved in terms of displacement or local stress fields, the global shear resultant extracted from solid models may remain unreliable and strongly dependent on the specific mesh configuration and element aspect ratio.

To further highlight the limitations and numerical challenges of traditional solid FEs widely used in commercial software, an additional study is carried out to assess the local equilibrium of an individual element within the structure. Figure 9 depicts the solid element selected for this evaluation, together with the stress components acting on each of its faces. Table 5 reports the resulting force components obtained by integrating the stresses over each face, along with the corresponding percentage error relative to the theoretical applied load. The results reveal important discrepancies: for ABAQUS solid models without reduced integration, the error reaches approximately 20%, decreasing to about 5% when reduced integration is employed. In contrast, the COMSOL solid solution exhibits an error of around 14%, further underscoring the different theories and numerical behaviors implemented in the two software tools.

2.1.2. Isotropic C-section beam

The second case deals with an isotropic unsymmetric C-section beam structure with clamped-free boundary conditions. Figure 10 shows the reference system and cross-section geometry. The structural dimensions and material parameters are specified as follows: $a_1 = 2\,\text{mm}$, $a_2 = 2.4\,\text{mm}$,

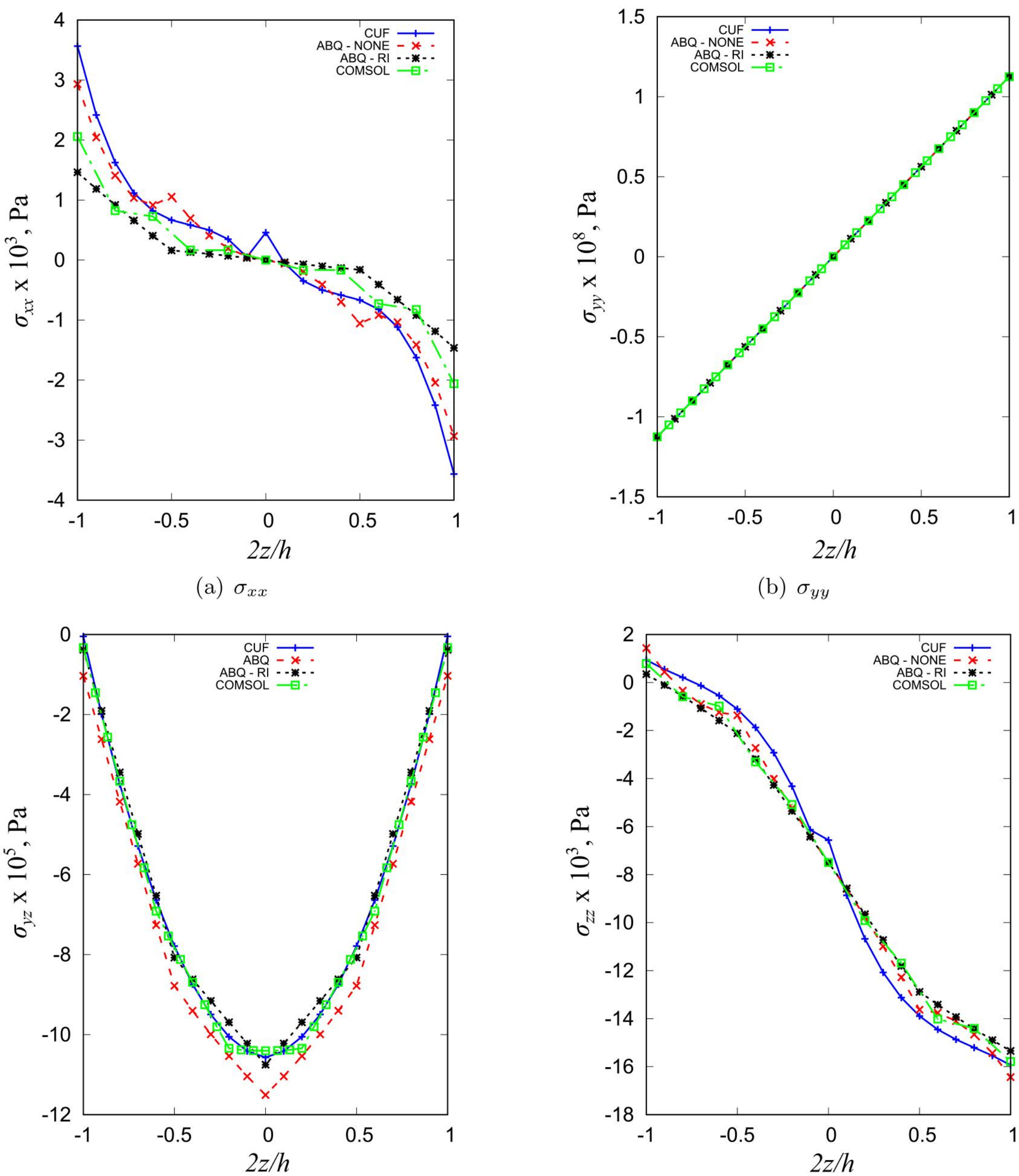

(a) σ_{xx} (b) σ_{yy}

(c) σ_{yz} (d) σ_{zz}

Figure 20. Comparison between CUF (AR = 10), ABAQUS (AR = 2) and COMSOL (AR = 1.2) for the through-the-thickness stress distributions for the isotropic square compact beam at the midspan.

$h = 3$ mm, $t = 0.2$ mm, $L = 0.1$ m, $E = 70$ GPa, and $\nu = 0.33$. Static analyses of this structure were carried out to evaluate the stress distribution induced by a concentrated load of $F = 4$ N applied at the free end on the top flange of the structure with the aim of comparing the different capabilities of ABAQUS and COMSOL solid models.

Table 6 gives the convergence analysis on the displacement at the loading point for various solid models, including the corresponding DOFs and maximum AR values. For this structure, the displacement evaluation also exhibits a marked sensitivity to the element aspect ratio and to the adopted mesh discretization.

The stress results for this benchmark are presented along three characteristic directions of the C-section, as indicated in Figure 10: along the web, through the thickness of the top flange, and along the width of the top flange. In addition, some specific points where the stresses are calculated are also included. These paths allow a detailed evaluation of the ability of solid formulations to reproduce stress distributions in regions dominated by bending, shear, and local deformations. Figure 11 shows the axial stress component, σ_{yy}, evaluated along the thickness (t). This component exhibits a rapid convergence, even when using relatively coarse solid meshes and elements with high aspect ratios, confirming that the axial response is generally less sensitive to mesh distortion in this configuration.

Figures 12 and 13 report the convergence behavior obtained with different solid models in ABAQUS, both with

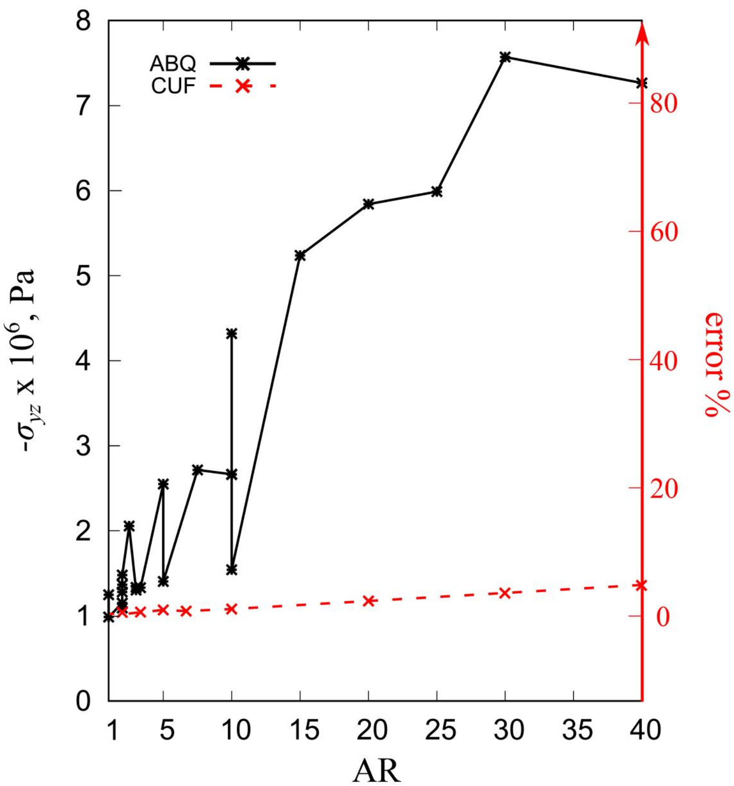

Figure 21. Aspect ratio influence on the σ_{yz} evaluated at midspan of the beam and at the Middle of the cross-section for CUF 1D and ABAQUS quadratic solid with full integration elements for an isotropic square compact structure.

full and reduced integration, along the web and along the top flange width. These comparisons highlight the influence of the integration scheme and mesh refinement on the accuracy of the stress predictions, particularly for the components that are more sensitive to kinematic effects.

In detail, the influence of the mesh discretization and element aspect ratio is illustrated in Figures 14, 15, and 16. These bar charts report the peak of stresses calculated along the web, through the thickness of the top flange, and along its width, for several mesh densities and AR configurations. The results clearly show that the accuracy of the stress predictions strongly depends on both parameters, with different levels of refinement and aspect ratio requirements depending on the specific stress component and position. In several cases, only highly refined meshes or suitably low AR values allow the solid formulations to capture the correct peak stress value.

3. Higher-order beam finite element formulation

To address the limitations encountered with solid elements in the previous section, 1D models based on the CUF are adopted [40]. CUF offers a general and systematic framework for deriving high-order 1D elements with 3D capabilities. Its key advantage lies in the separation of variables: the displacement field is expressed as the product of axial shape functions and cross-sectional expansion functions. Within this framework, the 3D displacement field is expressed as:

$$\boldsymbol{u}(x,y,z) = N_i(y)F_\tau(x,z)\boldsymbol{q}_{\tau i}, \qquad \tau = 1, ..., M \qquad i = 1, ..., N_n^{1D} \tag{8}$$

where F_τ stand for expansion functions defined over the cross-section, $\boldsymbol{q}_{\tau i}$ are the generalized displacement vector, M is the number of terms of the expansion, and the repeated index τ stands for summation. This structure allows to possible to assign different approximation orders to different directions. Therefore, the axial direction can be modeled with a simple, low-order interpolation, whereas the cross-section can be enriched to accurately capture deformation patterns, shear stresses, and local 3D phenomena. In practice, CUF-based 1D models concentrate computational resources exactly where they are most needed, achieving high-fidelity in the most critical directions without inheriting the computational burden of a full 3D mesh. This flexibility is precisely what enables CUF 1D models to retain solid-like accuracy even in geometries where traditional solid elements become inefficient or unreliable. Specifically, the parameters F_τ and M are user-defined inputs that determine the structural theory adopted in the model. In this work, Lagrange Expansion (LE) models, based on Lagrange polynomials to derive higher-order 1D theories are used [41]. An isoparametric formulation is employed to handle arbitrary geometries, with LE functions serving as F_τ over the beam cross-section. For clarity, the nine-point Lagrange polynomials (L9) and sixteen-point Lagrange polynomials (L16) are adopted for the cross-sectional approximation, whereas classical four-nodes 1D FEs (B4) with a cubic approximation along the beam axis are used for the axial discretization. Figure 17 shows the mesh discretization using CUF 1D elements.

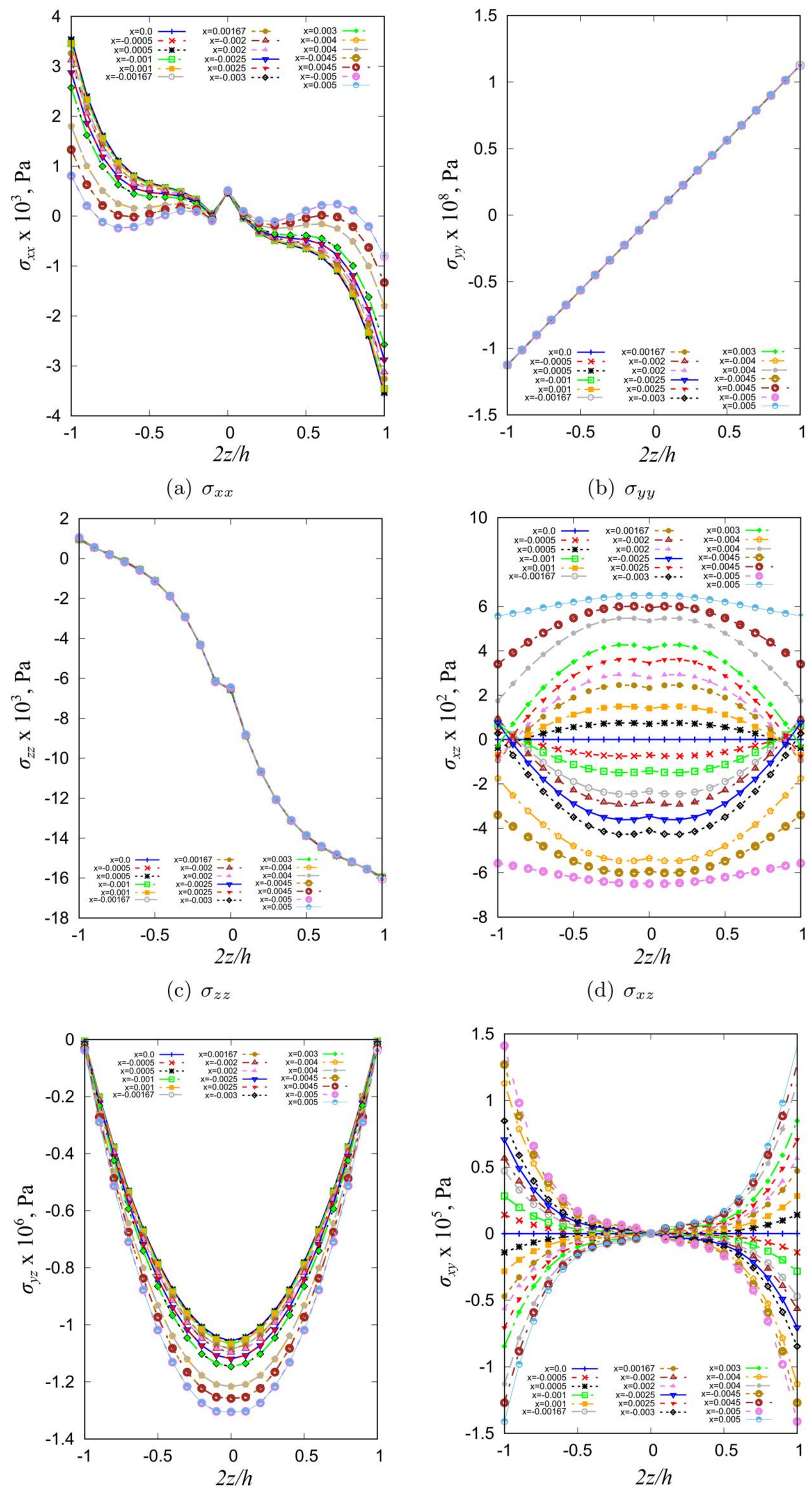

(a) σ_{xx} (b) σ_{yy}

(c) σ_{zz} (d) σ_{xz}

(e) σ_{yz} (f) σ_{xy}

Figure 22. Through-the-thickness stress distributions evaluated at various longitudinal positions (*x*-locations) at the midspan of the isotropic square compact beam using the CUF 1D.

Table 11. Equilibrium evaluation using CUF 1D at the considered single element. The percentage error reported in the table is computed with respect to the theoretical pressure resultant of 0.60 N applied to this element.

Model	$T_{\sigma^1_{xz}}$	$T_{\sigma^2_{xz}}$	$T_{\sigma^1_{yz}}$	$T_{\sigma^2_{yz}}$	$T_{\sigma^1_{zz}}$	$T_{\sigma^2_{zz}}$	Resultant [N]	Error %
125B4 + 4LE9	0.0104	0.0069	−0.2936	0.0079	−0.3815	−0.6833	−0.60	0.00

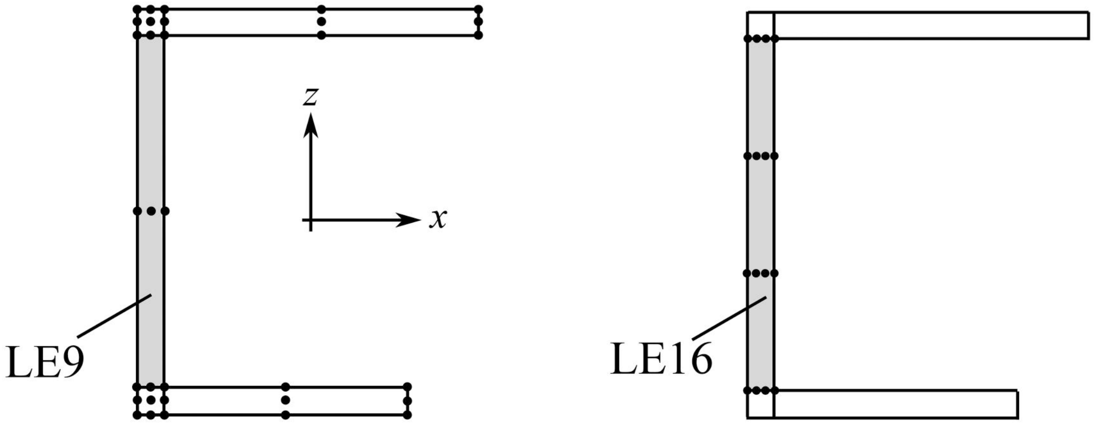

Figure 23. Cross-section discretization using LE9 or LE16 lagrange polynomials for the unsymmetric open-section beam structure.

Table 12. Displacement values at the loading point using various CUF 1D models for the isotropic C-section beam structure.

Model	AR	DOFs	$u_z \times 10^{-2}$ [m]
10B4 + 5LE9	50	3069	−1.660
10B4 + 13LE9	50	7533	−1.671
10B4 + 30LE9	100	14415	−1.673
10B4 + 5LE16	50	5952	−1.667
10B4 + 30LE16	100	29946	−1.678
20B4 + 5LE16	25	11712	−1.671
20B4 + 30LE16	50	58926	−1.683
30B4 + 30LE16	33.33	87906	−1.683
100B4 + 30LE16	10	290766	−1.683

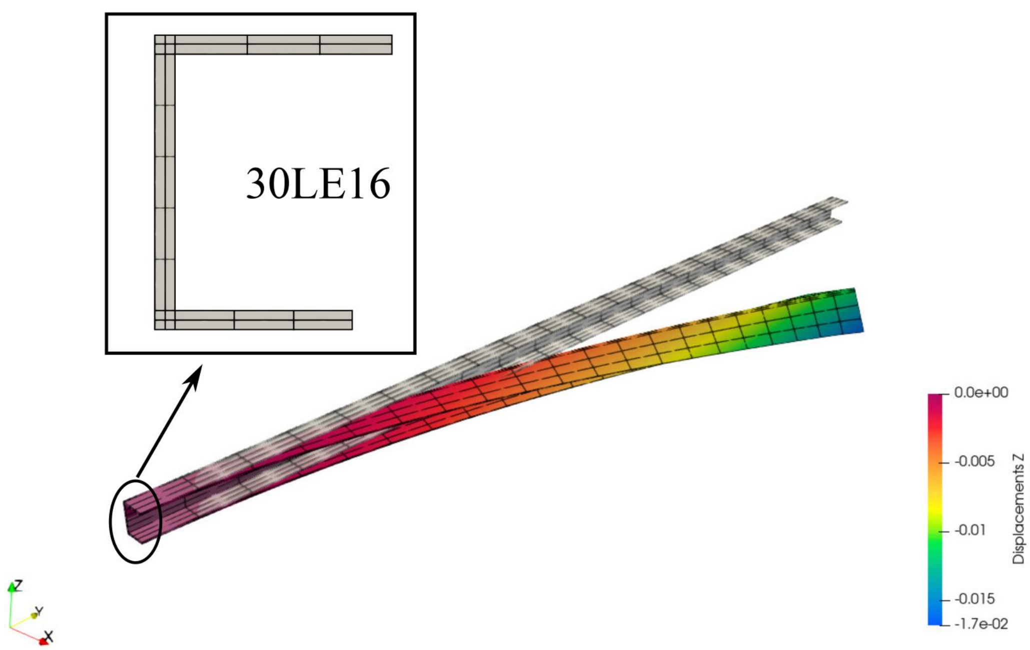

Figure 24. Deformed configuration of the isotropic cantilever beam with C-section subjected to a concentrated load. 20B4 + 30LE16 model.

For a beam model, the variations of the internal and external work are expressed in terms of FNs of the stiffness matrix and external force vector as follows:

$$\begin{aligned} \delta L_{int} &= \int_V \delta \boldsymbol{\epsilon}^{\mathrm{T}} \boldsymbol{\sigma} \ dV = \delta \boldsymbol{q}_{sj}^{\mathrm{T}} \boldsymbol{K}^{ij\tau s} \boldsymbol{q}_{\tau i} \\ \delta L_{ext} &= \delta \boldsymbol{q}_{sj}^{\mathrm{T}} \boldsymbol{p}_{sj} \end{aligned} \tag{9}$$

In a compact notation, the FN of the stiffness matrix for a beam model is written as [31]:

$$\boldsymbol{K}^{ij\tau s} = \int_V F_s(x,z) N_j(y) \boldsymbol{b}^{\mathrm{T}} \boldsymbol{C} \ F_\tau(x,z) N_i(y) \boldsymbol{b} \ dV \tag{10}$$

Consider the following two terms in the case of a beam:

$$\begin{aligned} K_{xx}^{ij\tau s} &= (\lambda + 2G) \int_l N_i(y) N_j(y) \ dl \int_A F_{\tau,x}(x,z) F_{s,x}(x,z) \ dA + \\ &+ \ G \int_l N_i(y) N_j(y) \ dl \int_A F_{\tau,z}(x,z) F_{s,z}(x,z) \ dA + \\ &+ \ G \int_l N_{i,y}(y) N_{j,y}(y) \ dl \int_A F_\tau(x,z) F_s(x,z) \ dA \\ K_{xy}^{ij\tau s} &= \lambda \int_l N_{i,y}(y) N_j(y) \ dl \int_A F_\tau(x,z) F_{s,x}(x,z) \ dA + \\ &+ \ G \int_l N_i(y) N_{j,y}(y) \ dl \int_A F_{\tau,x}(x,z) F_s(x,z) \ dA \end{aligned} \tag{11}$$

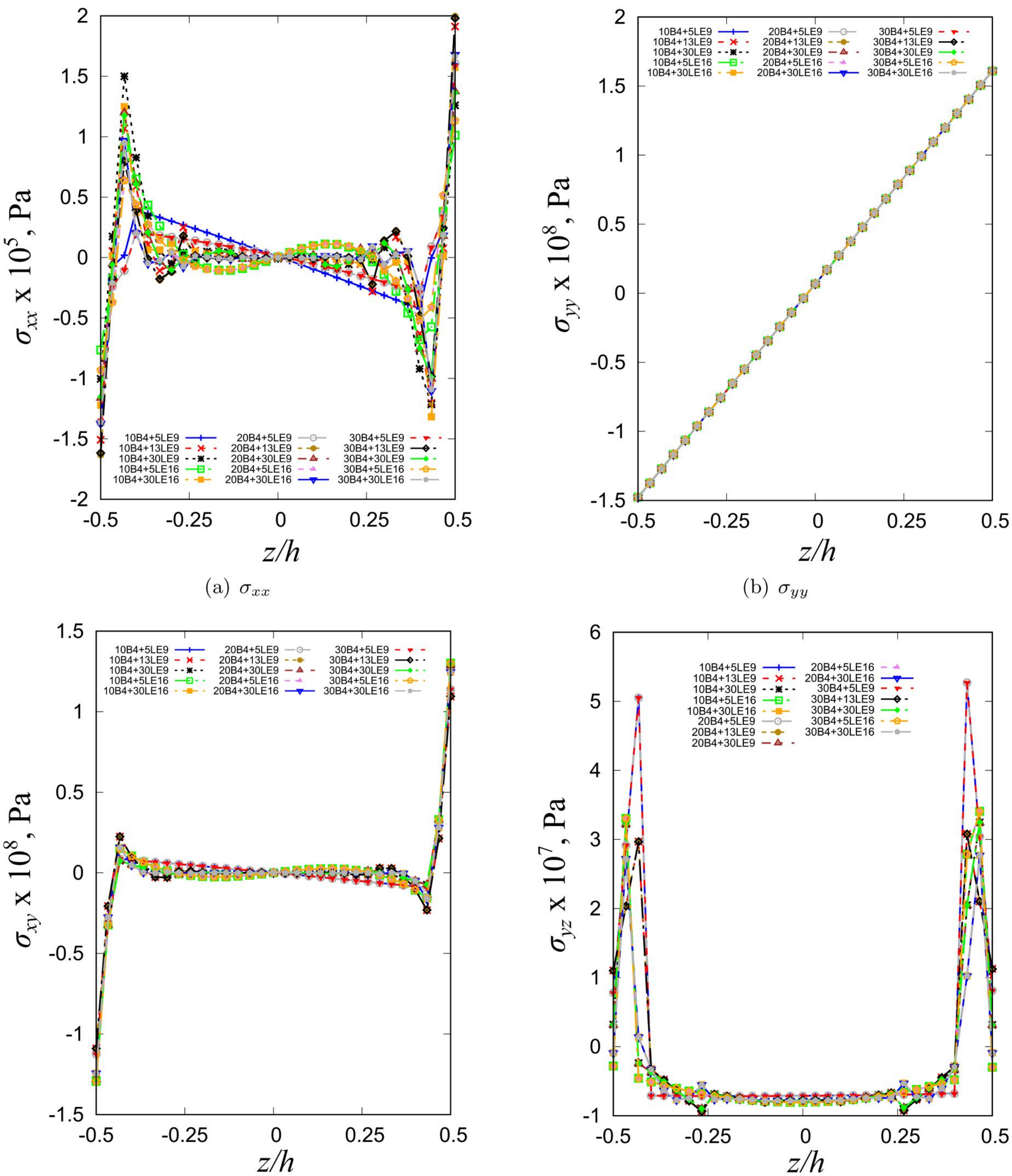

(a) σ_{xx} (b) σ_{yy}

(c) σ_{xy} (d) σ_{yz}

Figure 25. Stress distributions for the isotropic C-section beam at the midspan of the beam and along the web using CUF 1D models.

From Eq. 11, it becomes clear that a fundamental distinction between solid and CUF beam formulations lies in the construction of the stiffness matrix. In fact, solid elements require a full 3D volume integration, whereas CUF 1D beam models exploit the separation of variable to decompose the 3D integral into a line integral along the beam axis and a surface integral over the cross-section. This property enables the model to enrich the cross-section kinematics while keeping the computational cost low. Moreover, this difference has important practical implications. Solid formulations are inherently sensitive to the element aspect ratio, an issue that becomes particularly severe in slender, thin-walled or composite structures. Achieving accurate results typically demands low aspect ratio elements, which in turn necessitate highly refined meshes. CUF 1D models behave very differently. Thanks to the explicit separation of kinematic functions in the three spatial directions, CUF beam elements can employ rich expansion functions over the cross-section while retaining independent, lower-order shape functions along the beam axis. This feature allows to capture complex

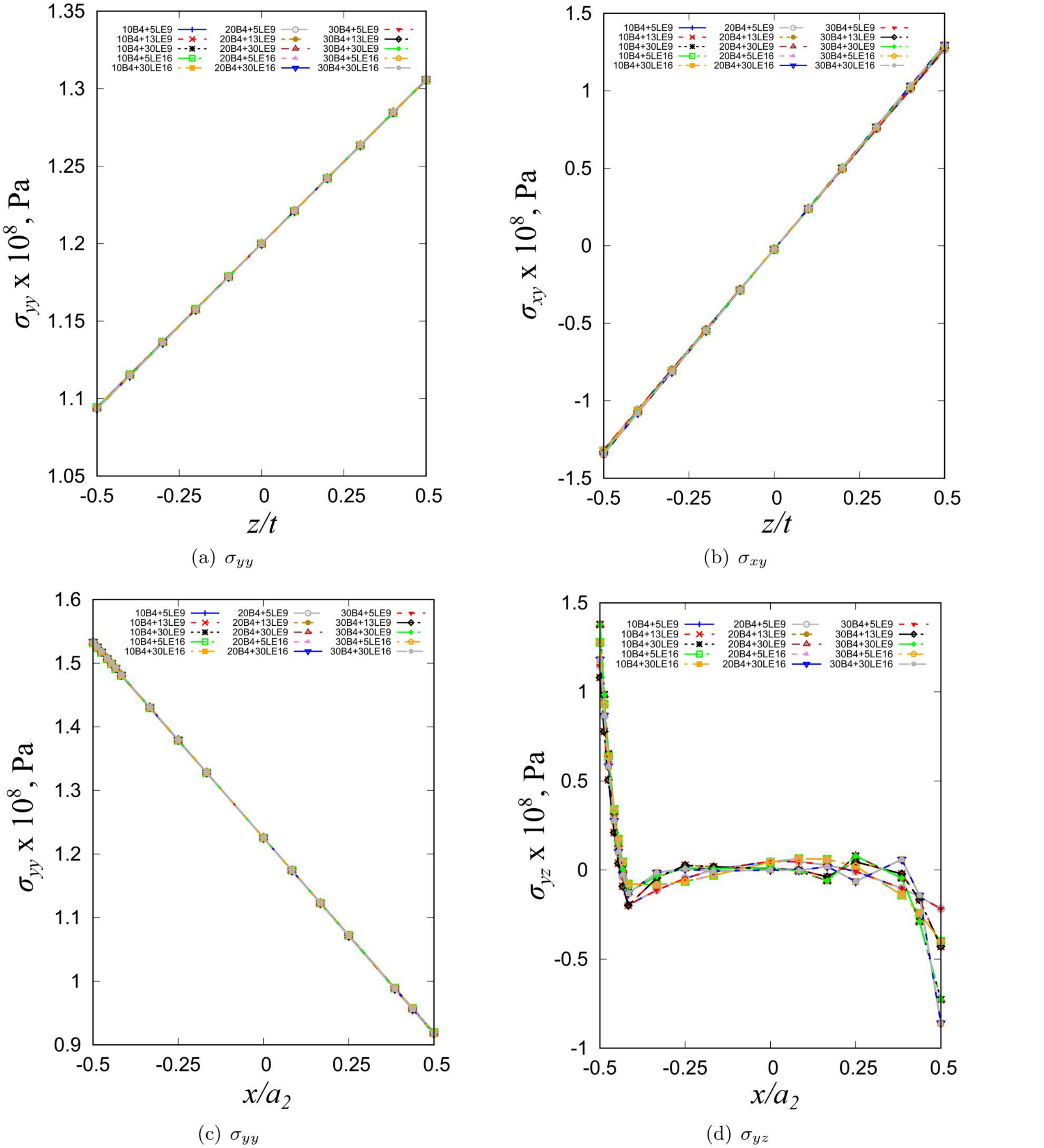

(a) σ_{yy} (b) σ_{xy}

(c) σ_{yy} (d) σ_{yz}

Figure 26. Stress distributions for the isotropic C-section beam at the midspan and along the thickness (a, b) and the width (c, d) of the top flange using CUF 1D models.

3D effects without the mesh refinement constraints that limit solid elements.

In CUF-based models, the stress field is reconstructed from an enriched displacement approximation. It reads:

$$\boldsymbol{\sigma} = \boldsymbol{C\epsilon} = \boldsymbol{Cb}N_iF_\tau\boldsymbol{q}_{\tau i} \tag{12}$$

Thanks to the presence of cross-sectional expansion functions, the model is able to capture detailed 3D stress states without requiring a fine discretization of the domain. This results in improved representation of through-the-thickness stress distributions, accurate prediction of transverse shear stresses, and reduced sensitivity to element aspect ratio.

3.1. Numerical results using CUF 1D models

A straightforward comparison between conventional solid models and higher-order 1D beam models is reported to demonstrate how the limitations of standard solid elements

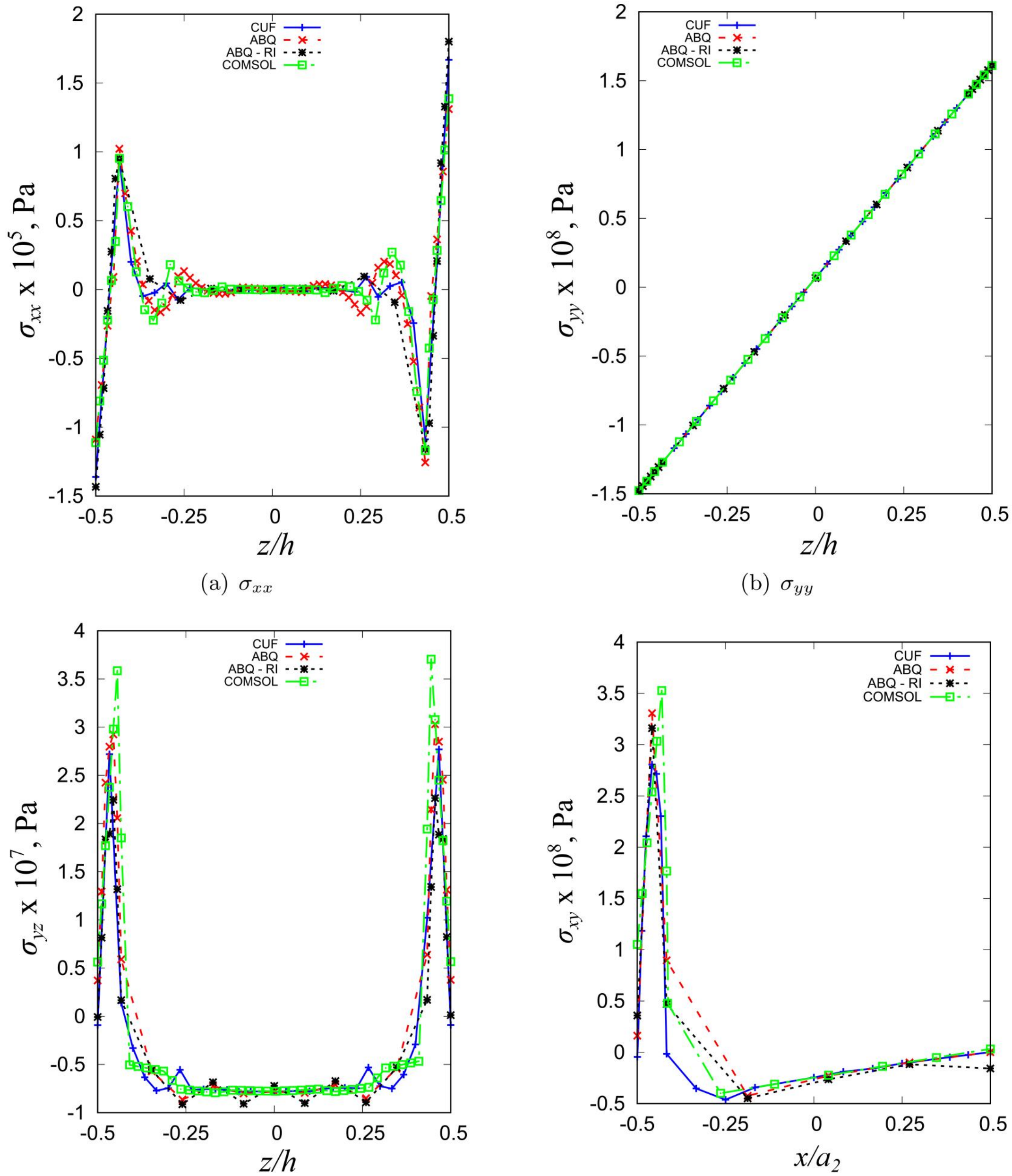

(a) σ_{xx} (b) σ_{yy} (c) σ_{yz} (d) σ_{xy}

Figure 27. Comparison between CUF (AR = 50), ABAQUS (AR = 5.55) and COMSOL (AR = 1.25) for the stress distributions along the web (a, b, c) and width (d) for the isotropic C-section beam at the midspan.

can be effectively overcome, achieving both greater computational efficiency and improved solution accuracy.

Regarding the first case, the CUF model is formulated using different B4 elements along the longitudinal axis and various LE9 and LE16 models across the beam cross-section in order to assess the influence of the kinematics. Table 7 reports the transverse displacement at the free end obtained using several CUF 1D models. The results suggest that a model with 10B4 + 1LE9 provides a convergent solution for the transverse displacement assessment. Figure 18 shows the deformed configuration, including the mesh discretization adopted.

A more detailed convergence analysis is then performed for the stress components, evaluated in the midspan cross-section of the beam. Figure 19, show that stress convergence requires a richer kinematic description than displacement convergence. While the axial stress, σ_{yy}, allows for accurate prediction even with models adopted for displacement evaluation, the complete 3D stress state requires a higher level of refinement. In particular, accurate evaluation of all stress components is achieved by employing 20B4 elements along the longitudinal axis combined with 2LE16 over the cross-section (5124 DOFs, AR = 2). This configuration ensures the correct representation of stress distributions and peak values along the cross-section, confirming that stress-based convergence criteria are more stringent than displacement-based ones. Figure 20 compares the CUF 1D results with those obtained using ABAQUS and COMSOL, showing

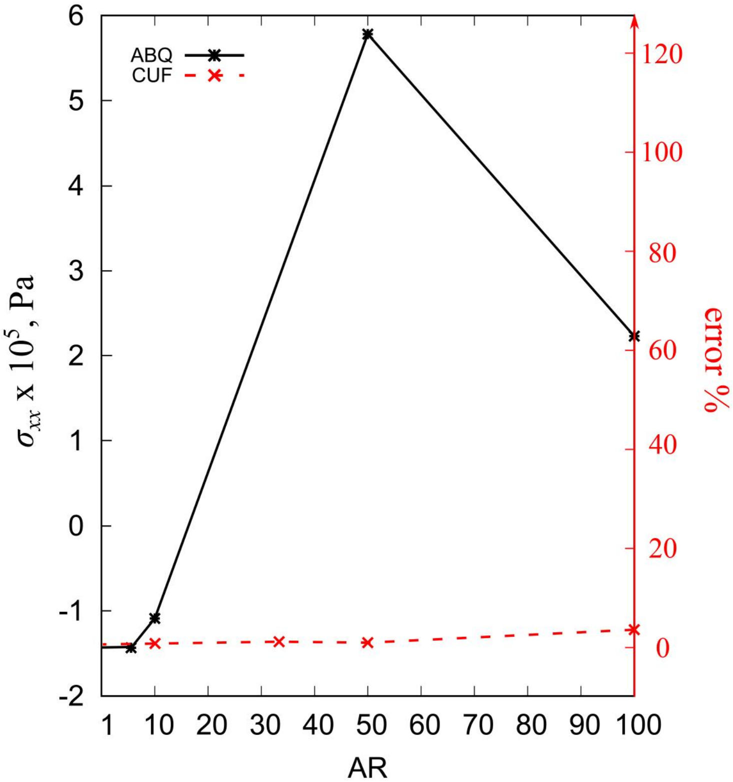

Figure 28. Aspect ratio influence on the σ_{xx} evaluated at midspan of the beam and at the bottom of the web for CUF 1D and ABAQUS quadratic solid with full integration elements for an isotropic C-section structure.

an excellent agreement. Notably, the CUF formulation attains this level of accuracy with a substantially lower computational cost, with reduction of 90.5 and 97.8% in the number of DOFs compared with the ABAQUS and COMSOL solid models, respectively, while avoiding the need for highly refined meshes or very low element aspect ratios. The influence of the aspect ratio is further highlighted in Figure 21, where the solid model exhibits a pronounced sensitivity to AR, leading to very large errors when elongated elements are used. In contrast, the CUF 1D formulation remains remarkably robust, maintaining low error levels even for high aspect ratios.

To further demonstrate the efficiency and reliability of the CUF 1D models, the same evaluation previously performed on the resultants at different beam sections is now repeated using the proposed refined beam formulations. Tables 8, 9, and 10 report the resultant obtained with the higher-order CUF 1D theories. The results clearly show that these models are able to reproduce the theoretical sectional resultants with remarkable accuracy at every section considered. This confirms that the enriched kinematics of the CUF beam formulations not only capture the correct stress trends, but also ensure full consistency with the applied loads, thereby guaranteeing the exact recovery of the expected sectional resultants. Additionally, Figure 22 depicts the through-the-thickness stress distributions of the isotropic compact square beam, evaluated at several longitudinal positions x at the midspan of the beam using the CUF 1D model. The plots highlight how the stress trends evolve as x varies, providing a more comprehensive characterization of the structural response than analyses restricted only to the middle of the section.

Finally, Table 11 demonstrates how the proposed beam formulation is also able to exactly recover the elastic equilibrium at the element level, unlike the solid element solutions, reported in Table 5. Moreover, the CUF 1D model achieves this accuracy with a significantly lower computational cost and without the strong sensitivity to element aspect ratio typically observed in solid formulations.

Next, the isotropic C-section beam is evaluated using the CUF 1D beam model. Figure 23 illustrates the cross-section discretization using the Lagrange theory.

Table 7 shows the convergence study on the transverse displacement at the loading point using various CUF 1D models. The convergent solution is obtained with the 20B4 + 30LE16 model, consisting of 58926 DOFs. The results further show that the CUF 1D formulations remain accurate and fully convergent even when very high aspect ratios (AR = 50) are used, confirming the robustness of the proposed approach (Table 12).

Figure 24 shows the deformed configuration of the C-section beam, including the contour plot of the transverse displacement and the convergent mesh discretization.

Figures 25 and 26 illustrates the convergence analysis of the stress field obtained with the CUF 1D formulation. These figures present the distribution of the stress components evaluated along the web, through-the-thickness, and along the width of the top flange. These results highlight the ability of the proposed beam model to accurately reproduce the 3D stress distribution with progressively more refined kinematics, confirming the robustness of the formulation in capturing both out-of-plane and in-plane stress variations, typical of thin-walled open-section beams.

Figure 27 reports the comparison between the CUF 1D, ABAQUS, and COMSOL solutions, showing a good agreement in the stress distributions. The results highlight that the proposed higher-order CUF beam models retain full accuracy even when using extremely high aspect ratio elements (AR = 50), whereas the solid formulations require lower aspect ratios to achieve convergence. Moreover, when comparing the converged solutions, the CUF 1D models achieve a reduction of approximately 74% in the number of DOFs relative to the ABAQUS solid model and about 77% relative to the COMSOL one. This confirms both the robustness and the computational efficiency of the CUF 1D approach in capturing 3D stress effects. Finally, the role of aspect ratio becomes even more evident in Figure 28, where the solid model shows marked sensitivity to AR, with errors growing dramatically as elements become more elongated. In contrast, the CUF 1D formulation remains highly robust, maintaining low error levels even at very high aspect ratios.

4. Conclusions

This work has examined the intrinsic limitations of solid finite elements (FEs) in the accurate evaluation of three-dimensional (3D) stress fields using the commercial software ABAQUS and COMSOL, with particular emphasis on their sensitivity to element aspect ratio (AR), dependence on mesh refinement, and difficulties in preserving local equilibrium. Through a series of benchmark analyses on compact and thin-walled isotropic structures, the study has highlighted how traditional solid formulations, despite their widespread use, often struggle to provide reliable stress predictions unless extremely fine meshes are employed. To overcome these issues, higher-order one-dimensional (1D) beam models with full 3D capabilities, developed within the Carrera Unified Formulation (CUF), have been proposed as an efficient and robust alternative. The following conclusions can be drawn:

- Solid finite elements exhibit a strong dependence on element aspect ratio. Even for simple geometries, high AR values lead to significant degradation of displacement and stress accuracy, particularly for the out-of-plane components. The reduced integration mitigate these issues compared to full integration, but remain sensitive to AR;
- The numerical results clearly show that stress convergence in solid models is highly problem-dependent. While axial stresses converge relatively quickly, shear stresses require very low AR values and dense meshes across the cross-section. This behavior is consistent across compact and thin-walled structures, confirming that solid formulations struggle to capture through-the-thickness stress distributions unless highly refined meshes are applied;
- Solid elements also exhibit difficulties in preserving local equilibrium. The shear resultants extracted from different cross-sections show large variations and significant deviations from the applied loads, even when displacement fields appear converged. This inconsistency highlights a fundamental limitation of solid formulations in reconstructing physically meaningful stress fields;
- Achieving accurate stress distributions with solid elements requires a dramatic increase in the number of degrees of freedom (DOFs). Reduced-integration elements improve convergence trends but do not eliminate AR-related inaccuracies. As a result, solid-based stress analyses often become computationally expensive and sensitive to discretization choices. In contrast, CUF-based higher-order 1D beam models provide accurate and robust stress predictions with a significant reduction of the computational cost. By enriching the cross-section kinematics through additional expansion functions, CUF models capture 3D stress states without the need for fine 3D meshes. The results demonstrate that CUF models remain insensitive to AR, preserve local equilibrium, and deliver consistent stress distributions across all test cases.

Overall, the study confirms that higher-order CUF 1D beam elements represent an effective and reliable alternative to traditional solid formulations for accurate stress analysis. Their ability to reproduce 3D stress fields with low computational effort makes them particularly suitable for slender and thin-walled structures, where solid elements often face severe numerical challenges. These results establish CUF-based models as efficient analysis tools and reliable references for verification and validation.

Future work will extend the present investigation to more complex structural configurations, including composite and sandwich beams, where accurate evaluation of 3D and interlaminar stresses is essential and solid elements often face even more severe numerical challenges. Additional developments will incorporate geometric nonlinearities to assess the behavior of slender structures under large displacements and rotations, as well as the performance of solid and CUF 1D models in highly nonlinear stress regimes. Finally, the methodology will be applied to rotating structures, where centrifugal stiffening, shear effects, and the accurate representation of stress fields are essential for reliable predictions.

Author contributions

CRediT: **Erasmo Carrera**: Conceptualization, Methodology, Software, Writing – review & editing; **Rodolfo Azzara**: Investigation, Visualization, Writing – original draft.

Disclosure statement

The authors declare that they have no conflict of interest.

References

[1] O.C. Zienkiewicz, and R.L. Taylor, The Finite Element Method for Solid and Structural Mechanics, Oxford, UK, Elsevier, 2005.

[2] T.J.R. Hughes, The Finite Element Method: Linear Static and Dynamic Finite Element Analysis, Mineola, New York, USA, Courier Corporation, 2012.

[3] S. Saloustros, M. Cervera, S. Kim, and M. Chiumenti, Accurate and locking-free analysis of beams, plates and shells using solid elements, Comput. Mech., vol. 67, no. 3, pp. 883–914, 2021. DOI: 10.1007/s00466-020-01969-0.

[4] Z. Luo, C. Liu, J. Li, X. Li, and X. Ji, Optimization of finite element mesh for residual stress measurement using contour method, Exp. Tech., pp. 1–22, 2025. DOI: 10.1007/s40799-025-00859-5.

[5] R.D. Cook, D.S. Malkus, and M.E. Plesha, Concepts and Applications of Finite Element Analysis, Hoboken, USA, John Wiley & Sons, 2007.

[6] J.R. Shewchuk, What is a good linear element? Interpolation, conditioning, and quality measures, 11th International Meshing Roundtable, {IMR} 2002, Ithaca, USA, 2002.

[7] P.M. Knupp, Achieving finite element mesh quality via optimization of the jacobian matrix norm and associated quantities. part II—A framework for volume mesh optimization and the condition number of the jacobian matrix, Int. J. Numer. Meth. Eng., vol. 48, no. 8, pp. 1165–1185, 2000. DOI: 10.1002/(SICI)1097-0207(20000720)48:8<1165::AID-NME940>3.0.CO;2-Y.

[8] J.C. Simo, and M.S. Rifai, A class of mixed assumed strain methods and the method of incompatible modes, Numer. Meth. Eng., vol. 29, no. 8, pp. 1595–1638, 1990. DOI: 10.1002/nme.1620290802.

[9] J.C. Simo, and F. Armero, Geometrically non-linear enhanced strain mixed methods and the method of incompatible modes, Numer. Meth. Eng., vol. 33, no. 7, pp. 1413–1449, 1992. DOI: 10.1002/nme.1620330705.

[10] T.J.R. Hughes, R.L. Taylor, and W. Kanoknukulchai, A simple and efficient finite element for plate bending, Numer. Meth. Eng., vol. 11, no. 10, pp. 1529–1543, 1977. DOI: 10.1002/nme.1620111005.

[11] K.J. Bathe, and E.N. Dvorkin, A four-node plate bending element based on Mindlin/Reissner plate theory and a mixed interpolation, Numer. Meth. Eng., vol. 21, no. 2, pp. 367–383, 1985. DOI: 10.1002/nme.1620210213.

[12] R.L. Taylor, P.J. Beresford, and E.L. Wilson, A non-conforming element for stress analysis, Numer. Meth. Eng., vol. 10, no. 6, pp. 1211–1219, 1976. DOI: 10.1002/nme.1620100602.

[13] T.J.R. Hughes, Generalization of selective integration procedures to anisotropic and nonlinear media, Numer. Meth. Eng., vol. 15, no. 9, pp. 1413–1418, 1980. DOI: 10.1002/nme.1620150914.

[14] J.C. Nagtegaal, D.M. Parks, and J.R. Rice, On numerically accurate finite element solutions in the fully plastic range, Comput. Methods Appl. Mech. Eng., vol. 4, no. 2, pp. 153–177, 1974. DOI: 10.1016/0045-7825(74)90032-2.

[15] D.S. Malkus, and T.J.R. Hughes, Mixed finite element methods—reduced and selective integration techniques: a unification of concepts, Comput. Methods Appl. Mech. Eng., vol. 15, no. 1, pp. 63–81, 1978. DOI: 10.1016/0045-7825(78)90005-1.

[16] D.S. Bombarde, L.N. Silla, S.S. Gautam, and A. Nandy, A comprehensive comparative review of various advanced finite elements to alleviate shear, membrane and volumetric locking, Arch. Computat. Methods Eng., vol. 31, no. 4, pp. 1979–2013, 2024. DOI: 10.1007/s11831-023-10050-x.

[17] A. Aguirre, R. Codina, and J. Baiges, Stress–displacement stabilized finite element analysis of thin structures using solid-shell elements, part I: on the need of interpolating the stresses, Finite Elem. Anal. Des., vol. 236, pp. 104168, 2024. DOI: 10.1016/j.finel.2024.104168.

[18] D. Bernoulli, De Vibrationibus et Sono Laminarum Elasticarum, Commentarii Academiae Scientiarum Imperialis Petropolitanae, 2017.

[19] L. Euler, De curvis elasticis. In: Methodus Inveniendi Lineas Curvas Maximi Minimive Proprietate Gaudentes, Sive Solutio Problematis Isoperimetrici Lattissimo Sensu Accepti, Bousquet, 1744.

[20] A. de Saint-Venant, Mémoire sur la flexion des prismes, J. Math. Pures Appl., vol. 1, pp. 89–189, 1856.

[21] A. de Saint-Venant, Mémoire sur la torsion des prismes, Académie Des Sciences de L'Institut Impérial de Frances., vol. 14, pp. 233–560, 1856.

[22] S.P. Timoshenko, On the correction for shear of the differential equation for transverse vibrations of prismatic bars, Philos. Mag., vol. 41, no. 245, pp. 744–746, 1921. DOI: 10.1080/14786442108636264.

[23] G.R. Cowper, The shear coefficient in Timoshenko's beam theory, J. Appl. Mech., vol. 33, no. 2, pp. 335–340, 1966. DOI: 10.1115/1.3625046.

[24] V. Berdichevsky, E. Armanios, and A. Badir, Theory of anisotropic thin-walled closed-cross-section beams, Compos. Eng., vol. 2, no. 5-7, pp. 411–432, 1992. DOI: 10.1016/0961-9526(92)90035-5.

[25] V.V. Volovoi, and D.H. Hodges, Theory of anisotropic thin-walled beams, J. Appl. Mech., vol. 67, no. 3, pp. 453–459, 2000. DOI: 10.1115/1.1312806.

[26] K. Washizu, Variational methos in elasticity and plasticity, In: International Series of Monographs in Aeronautics and Astronautics, 1968.

[27] E. Carrera, and M. Petrolo, Refined one-dimensional formulations for laminated structure analysis, AIAA J., vol. 50, no. 1, pp. 176–189, 2012. DOI: 10.2514/1.J051219.

[28] R.K. Kapania, and S. Raciti, Recent advances in analysis of laminated beams and plates. Part I: shear effects and buckling, AIAA J., vol. 27, no. 7, pp. 923–935, 1989. DOI: 10.2514/3.10202.

[29] V.V. Novozhilov, Theory of Elasticity, Pergamon, Elmsford, 1961.

[30] E. Carrera, I. Elishakoff, and M. Petrolo, Who needs refined structural theories? Compos. Struct., vol. 264, pp. 113671, 2021. DOI: 10.1016/j.compstruct.2021.113671.

[31] E. Carrera, M. Cinefra, M. Petrolo, and E. Zappino, Finite Element Analysis of Structures through Unified Formulation, John Wiley & Sons, Chichester, West Sussex, UK, 2014.

[32] E. Carrera, G. Giunta, and M. Petrolo, Beam Structures: Classical and Advanced Theories, Chichester, West Sussex, UK, John Wiley & Sons, 2011.

[33] A. Pagani, A. Racionero Sánchez-Majano, and M. Petrolo, Influence of structural theories on optimal fiber distributions in tow-steered composites considering local strain and stress, Aerotec. Missili Spaz., vol. 105, no. 2, pp. 207–225, 2026. DOI: 10.1007/s42496-025-00275-3.

[34] E. Scano, D. Carrera, and M. Petrolo, Use of the 3D equilibrium equations in the free-edge analyses for laminated structures with the variable kinematics approach, Aerotec. Missili Spaz., vol. 103, no. 2, pp. 179–195, 2024. DOI: 10.1007/s42496-023-00177-2.

[35] R. Azzara, E. Carrera, M. Filippi, and A. Pagani, Time response stress analysis of solid and reinforced thin-walled structures by component-wise models, Int. J. Str. Stab. Dyn., vol. 20, no. 14, pp. 2043010, 2020. DOI: 10.1142/S0219455420430105.

[36] R. Azzara, M. Filippi, and A. Pagani, Variable-kinematic finite beam elements for geometrically nonlinear dynamic analyses, Mech. Adv. Mater. Struct., vol. 30, no. 20, pp. 4146–4154, 2023. DOI: 10.1080/15376494.2022.2091185.

[37] A. Racionero Sánchez-Majano, R. Masia, A. Pagani, and E. Carrera, Microscale thermo-elastic analysis of composite materials by high-order geometrically accurate finite elements, Compos. Struct., vol. 300, pp. 116105, 2022.

[38] R. Azzara, M. Filippi, and E. Carrera, Coupled thermoelastic transient analyses of truss-like structures via high-fidelity beam models, J. Therm. Stresses., vol. 48, no. 12, pagespp. 1529–1547, 2025. DOI: 10.1080/01495739.2025.2518459.

[39] R. Azzara, M. Filippi, M. Petrolo, R. Ricci, and G. Zecchin, Improved aeroelastic analysis framework to assess shear and cross-section deformability effects on static aeroelastic response, Proc. Inst. Mech. Eng. Part G: J. Aerospace Eng. 2026. DOI: 10.1177/09544100261437337.

[40] E. Carrera, A. Pagani, M. Petrolo, and E. Zappino, Recent developments on refined theories for beams with applications, Mech. Eng. Rev., vol. 2, no. 2, pp. 14-00298–14-00298, 2015. DOI: 10.1299/mer.14-00298.

[41] E. Carrera, and M. Petrolo, Refined beam elements with only displacement variables and plate/shell capabilities, Meccanica., vol. 47, no. 3, pp. 537–556, 2012. DOI: 10.1007/s11012-011-9466-5.